Ocean Engineering 291 (2024) 116243

Contents lists available at ScienceDirect

Ocean Engineering

journal homepage: www.elsevier.com/locate/oceaneng

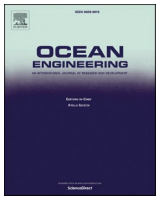

Experimental investigation of wave severity and mooring pretension on the operability of a moored tanker in a port terminal

H.S. Abdelwahab [a,b], L. Pinheiro [c], J.A. Santos [a,d], C.J.E.M. Fortes [c], C. Guedes Soares [a,*]

[a] Centre for Marine Technology and Ocean Engineering (CENTEC), Instituto Superior Técnico, Universidade de Lisboa, Lisbon, Portugal
[b] On leave from the Department of Naval Architecture and Marine Engineering, Alexandria University, Egypt
[c] Laboratório Nacional de Engenharia Civil (LNEC), Lisbon, Portugal
[d] Instituto Superior de Engenharia de Lisboa (ISEL), Instituto Politécnico de Lisboa, Portugal

ARTICLE INFO

Handling Editor: Prof. A.I. Incecik

Keywords:
Physical modelling
Ship operability
Port downtime
Ship motions
Moored ship
Mooring pretension

ABSTRACT

This paper investigates the influence of sea severity and mooring line pretension configuration on the operability of a moored vessel at a modified berthing site inside a port. A physical model was constructed to replicate the new layout of the port of Leixões in Portugal, including bathymetry and a future 300 m extension of Leixões' north breakwater. A tanker ship model was tested with novel custom-made mooring system simulators for two fenders and four mooring lines under various offshore sea states and pretension configurations. The experiments focus on acquiring wave measurements at multiple spots within the port, ship motions, and loads on lines and fenders. The data is analysed in time and frequency domains to examine the relationship between waves, motions, and loads. The results are then compared to standard operational thresholds to estimate downtime and operability for cargo loading operations. The analysis of the results yields several conclusions. It is recommended to use the zero-peak amplitudes in conjunction with the maximum peak-to-peak amplitudes to ensure accurate operability analysis. The application of small-scale physical modelling for a moored tanker in Leixões port is a useful tool not only for investigating the feasibility of port modifications in the existing sheltering structures but also for analysing additional soft countermeasures to strengthen operational conditions at the berth. It also provides site-specific experimental data that may help to develop site-specific safety criteria. The applied mooring simulators help to reduce physical model costs.

1. Introduction

The enormous growth in trade demand in recent years has encouraged technological advances in ship design and construction to focus on building larger vessels to decrease the transport costs of goods over long distances. The duration of the sea voyage, as well as the time spent at cargo-handling terminals, are significant elements that may influence transport costs. Large vessels, such as tankers and liquefied natural gas (LNG) ships, tend to be moored at cargo-handling facilities such as offshore terminals or buoys located near deep water, hence more exposed to severe sea waves or swells. They can also be moored at terminals often located near the entrance of sheltered ports away from the large ocean waves; nevertheless, they may be subjected to resonant behaviour, especially when under the action of low-frequency waves, whereas the eigen periods of moored ships or harbours normally correspond to the long-period gravity waves. Increasing the depth and width of the entrance channels to accommodate these large vessels may further expose the berth to more complex wave conditions. Large ship displacement and low mooring stiffness provide a long natural period for horizontal motions, whereas damping for these responses is minimal.

Large ship motions induced by swell and long waves, as well as wind, current, and passing ship effects, may hinder ship mooring and cargo handling operations and, consequently, reduce berth efficiency. In the worst-case scenario, they can break mooring lines, which potentially leads to fatal accidents for the crew, environmental impacts and damages to the ship, bollards, fenders, terminals, and cargo handling equipment because of the vessel's collision or drift. Determining the operational parameters of any terminal requires knowledge of the site-specific environmental conditions to incorporate into coupled hydrodynamic simulations considering the complex nonlinear mooring behaviour, finally leading to an increase in the port's capacity.

In the case of the oil terminal in the port of Leixões in Portugal,

* Corresponding author.
E-mail address: c.guedes.soares@centec.tecnico.ulisboa.pt (C. Guedes Soares).

https://doi.org/10.1016/j.oceaneng.2023.116243
Received 31 May 2023; Received in revised form 29 October 2023; Accepted 2 November 2023
Available online 3 December 2023

moored tanker ships experience frequent downtime due to the risk of mooring system failure caused by excessive large motions at severe sea states (Veloso-Gomes et al., 2005). Some studies concentrated on investigating minor changes at this berthing site to enhance operational efficiency (Rosa-Santos et al., 2008, 2010; Rosa-Santos and Taveira-Pinto, 2013). This study, on the contrary, focuses on implementing significant modifications, such as extending the existing north breakwater and increasing water depth in the berth area, as approved by the port authority APDL (2016) to accommodate both larger and additional vessels. In this study, the operational conditions of a moored tanker in the port of Leixões at the oil terminal facility, including the new extension of the north breakwater, are investigated experimentally under diverse testing circumstances. The primary goal is to obtain wave elevations and directions at various locations within the port, the ship motions in six degrees of freedom (DOF), and the loads on mooring lines and fenders under various pretension configurations and wave climate conditions outside the port. The study then examines the relationship between them and investigates the influence of sea severity and pretension configurations on the operability of a tanker moored at the newly modified berth.

The novel aspects of the presented experimental study are as follows. The study introduces a novel, custom-made and cost-effective mooring solution, as an alternative to the traditional mooring equipment, which has been extensively employed in most testing facilities when simulating nonlinear moored systems with physical models. The experimental investigation reveals that the north breakwater extension significantly reduces wave heights compared to the previous breakwater configuration, nevertheless, the efficiency might be reduced when under low-frequency waves. The results obtained in the experimental campaign can play a crucial role when validating numerical models of moored ships. Furthermore, they can be valuable for guiding future experimental studies and establishing specific limiting criteria, tailored to the Leixões oil terminal, for short and long waves, vessel motions, and mooring loads, rather than relying on generic or standard criteria. The study concludes that increasing pretensions should not be used blindly as a countermeasure to enhance operability without first ensuring that the mooring arrangement is feasible for safe operation. The study also advocates using zero-peak amplitudes in conjunction with maximum peak-to-peak amplitudes to obtain correct operability based on a comprehensive mono-parametric downtime assessment.

The paper is organized as follows: Section 2 presents an extensive review of the moored ship problem in ports. First, it starts with discussing ship mooring accidents globally and how competent authorities respond. After that, review the feasible alternatives for safely moored ships in port. Then, discuss the typical approaches for assessing moored ship response in ports. Finally, it summarises the safe mooring criteria for moored tankers. Section 3 describes the study area, testing facility, and physical model layout. The experimental equipment is then described in detail, including the ship model, wave measurement system, mooring system, and motion capture system. The testing conditions and procedure are also summarized, followed by a description of the data analysis techniques used. Section 4 investigates the Leixões oil terminal's tranquillity as well as a moored tanker's operability under various testing parameters. Finally, several conclusions are drawn in Section 5.

2. Review of moored ship problem

2.1. Global mooring-related accidents

The number of cases in which large vessels exceed available berths and the ship's bow or stern is overhung has increased, making proper attachment of the mooring lines to the ship difficult (Kim et al., 2019). In addition, many terminals are still underequipped to manage the mooring of large new ships, and accidents caused by mooring system failure are becoming more frequent. According to a 20-year survey, mooring ropes and wires cause 95% of personal injury accidents (53% by a broken line and 42% by line slipping off drum ends or bitts), with approximately 60% of these injuries occurring during typical mooring operations (UK P&I Club, 2009). Another inspection of 373 ships revealed that 14% of the mooring arrangements were unsatisfactory (UK P&I Club, 2016). The Australian Maritime Safety Authority declared 227 mooring-related accidents based on a 5-year survey, with 22% of these accidents having injuries (AMSA, 2015). A deck officer suffered severe head injuries in 2015 when he was hit by a broken mooring line during a berthing operation at the South Hook LNG terminal in the United Kingdom (MAIB, 2017). A mooring line snapback caused one fatality in Canada when the line got free from being stuck on a fender (TSB, 2018).

The Massachusetts Port Authority's inability to provide proper berthing arrangements caused a mooring bollard to fail when overloaded with multiple lines, causing a moored container ship to drift, and hit a nearby pier in 2017. Ship and terminal damage cost $1 million (NTSB, 2018). A drill ship crashed into a bridge in Spain after breaking its moorings during a heavy storm, causing socioeconomic concerns in the region (Figuero et al., 2018). In 2020, a severe storm forced a tanker away from a Danish oil terminal's jetty. The mooring lines released uncontrollably when the aft mooring winch exceeded its breaking load. Consequently, the ship's manifold and the terminal's loading arms were damaged, causing a significant oil spill (DMAIB, 2020).

The increasing trend of mooring-related accidents at the Australian port of Port Hedland (more than 20% of all marine accidents) motivated the port authority to impose new mandatory mooring requirements on all vessels entering the port and their crew to reduce accident frequency and address the root causes (BHP, 2021; PPA, 2021). Recently, amendments and updates to Safety of Life at Sea (SOLAS) Chapter II-1/3–8 were adopted to enhance ship mooring safety (DNV, 2020). New guidelines were adopted for the design of mooring arrangements, selection of safe mooring equipment and fittings (MSC, 2020a), inspection and maintenance of mooring equipment including lines (MSC, 2020b), and shipboard towing and mooring equipment (MSC, 2020c). Regardless of experience, the risks connected with mooring operations are extremely serious. The frequency and consequences of the above-mentioned mooring-related accidents around the world highlight the need for proactive studies into the behaviour of moored ships at cargo-handling terminals to prevent mooring-related accidents.

2.2. Feasible alternatives for a safely moored ship

The reduction of the moored ship motions is critical for increasing berth operability and safety and minimizing operating costs and environmental hazards (Rosa-Santos et al., 2014). Two feasible alternatives can be applied to avoid or mitigate the resonance phenomena that result in undesirable large motions of moored ships. Firstly, adjusting the wave environment to reduce wave energy and its impact on the ship at the berthing site. Secondly, tuning the dynamic moored system to establish safe natural periods of motion that do not coincide with the exciting wave period. Achieving the latter can involve adjustments to the mooring configuration, which may be an inexpensive solution compared to the former which requires a long-term process of constructing new sheltering structures or modifying existing ones (Sakakibara and Kubo, 2008a).

2.2.1. Mitigation of wave energy inside ports

The design of the port and its structures may influence the environmental conditions and consequently, it may affect the forces exerted on the moored ships (OCIMF, 2018). Rusu and Guedes Soares (2011) studied the wave conditions at the entrance of Leixões port. Bellotti (2007) studied numerically the effect of various port entrance layouts on internal port resonance. McComb et al. (2009) investigated several alternatives of breakwater structure to limit swell and long-wave propagation into a port. Studies show that sheltering structures, such as breakwaters, may reduce the wind waves, currents, swell and long

waves by dissipating part of their energy. However, they may occasionally provide limited improvement in berth operability (Ahuja et al., 2010a, 2010b; Taveira-Pinto et al., 2008; Van der Molen et al., 2016).

2.2.2. Refinements in conventional mooring system

To improve operational efficiency and safety while employing conventional mooring for large ships, various modifications can be investigated to select the best mooring system in a site-specific study. Many of these modifications are based on decreasing the ship's response by applying further restrictions to prevent it from acquiring momentum. Modifications may include adding new lines, fenders, and pretensions, or replacing mooring elements with those that have a better load-deformation relationship. Kubo et al. (2001) declared that under combined wind and wave action, tension and slack mooring can be suitable for large and small ships, respectively. Van der Molen et al. (2006) demonstrated that tightening or slackening mooring lines can reduce ship response to low-frequency waves by shifting the dynamic system's natural frequency away from the harbour oscillation frequency. However, the limitations of applying higher pretensions include the handling of the mooring lines, mooring bit strength, forces on quick-release hooks and excessive fender compression or line tension. Therefore, alternative countermeasures to avoid resonance would be more convenient.

Sakakibara and Kubo (2008a) proved that a combined modification in the load-deformation characteristics and mooring arrangement is an effective countermeasure for restraining large and low-frequency ship motions under rough weather. However, it is critical to ensure that modifications to the mooring system's characteristics transform the asymmetrical system into a symmetrical or weak asymmetrical system by having the ratio of spring constants between fenders and lines close to one (Sakakibara and Kubo, 2008b). This can be attained by switching from synthetic fibre to wireline as well as from hard buckling to soft pneumatic fender. A good fender, in general, absorbs a considerable amount of energy while providing a low reactive load to the quay or the ship (Villa-Caro et al., 2018). Rosa Santos et al. (2014) investigated experimentally the combined effect of modifying the fenders' friction coefficient and line pretension on the motions and mooring loads of a tanker moored in Leixões port. Results indicate that their contribution to improving operational and safety conditions decreases in rough waves.

2.2.3. Implementing innovative mooring technologies

Some studies focused on modifying the mooring characteristics by installing mooring winches on the berth. For example, Yoneyama et al. (2004) experimentally investigated computer-controlled hybrid mooring winches linked to wave height and ship motion measuring devices to forcefully change the natural period of the dynamic moored system by automatically adjusting the ratio between the mooring lines and tail based on recorded data. Thus, the mooring stiffness automatically changes between soft and hard mooring to reduce the low-frequency motions. Ahuja et al. (2010b) found that adding constant tension shore-based winches with mooring lines instead of building a new breakwater structure improved operation efficiency and avoided morphological influence on an Indian jetty LNG terminal. Van der Molen et al. (2016) assessed numerically numerous mooring configurations for a bulk carrier against the expansion of a breakwater to mitigate long-wave problems in an Australian port. Results show that installing a combination of pneumatic fenders and constant tension winches or nylon breast lines leads to great reductions in ship responses.

Innovative mooring systems were developed recently to overcome large vessel motions, enhance operability, and save time, money, and the environment. A variety of active damping motion technologies are currently available in the market as an alternative to conventional mooring. The vacuum-based automatic mooring system uses vacuum pads for mooring attachment linked to flexible hydraulic arms to provide stiffness and damping in the horizontal plane to restrict the moored ship's surge, sway, and yaw motions. It can either be ship-based such as Iron Sailor (Villa-Caro et al., 2018) or shore-based such as QuaySailor or MoorMasters (Cavotec, 2004; Montgomery, 2013). Unlike the former, which is activated by extending out the pads through doors in the hull to attach to a steel plate on the berth, the latter can be installed on a quayside or pontoons and does not require specific ship installations. De Bont et al. (2010) studied the efficacy of utilizing MoorMasters units instead of conventional mooring lines to mitigate the surge response of a moored containership in the Port of Salalah. Kim et al. (2014) used full-scale trials to demonstrate the feasibility of a vacuum-based automatic mooring system in reducing heave, surge and sway motions between two ships under significant levels of waves and winds.

Van der Burg (2011) proposed another active motion damping system, ShoreTension®, which is a standalone hydraulically controlled piston that can be placed on the quayside between a quay bollard and a stiff mooring line connected to the ship's mooring bitts to automatically maintain the lines taut in extreme wave conditions while fender friction increases. When tension is high, the mechanism releases the mooring line to absorb peak loads without exceeding the minimum breaking load (MBL). This prevents line failure due to loading/unloading, and tidal level changes. The hydraulic piston might serve as a weak tail during swells (Van Deyzen et al., 2014). Van der Burg (2011) showed that ShoreTension® significantly reduces motions and mooring loads on a moored LNG carrier under passing ship effects and combined wind and wave action. Full-scale measurements in Portugal show that ShoreTension® can reduce the response of a moored container ship in Sines port under severe waves (Van Deyzen et al., 2015). Van Deyzen et al. (2014) found that both MoorMasters and ShoreTension® systems significantly decrease the horizontal responses of a container ship moored at an exposed jetty when compared to a conventional mooring system under wind and wave action.

The DOCK LOCK® automatic mooring system is a shore-based active motion damping system similar to MoorMasters, however, it provides the mooring attachments through electronically controlled magnetic pads. (Van Reenen, 2013). The Dock Lock® system is now utilized on bunker vessels that transfer fuel to ships in port, but it may also be used in ports to reduce ship response due to long waves (Van der Molen et al., 2016). Himanen (2016) noted that both magnetic and vacuum-based systems may not fit ports with significant currents as they do not allow any lateral movement. Another shore-based mooring technology to speed up terminal operations is mechanical arm mooring, which requires a piece male in the ship side to connect besides accurate alignment between the ship and quay (Villa-Caro et al., 2018).

Sakakibara and Kubo (2007) presented a monitoring technology that provides on-site assessment for loads on pneumatic fenders and alerts at critical conditions. Some harbours applied a weather forecast system to evacuate ships from piers, as an alternative to the above-mentioned mooring technologies, when severe weather is predicted (Shiraishi, 2009). However, inaccurate wave forecasts may still cause dangerous mooring issues (Lee et al., 2021). Although various novel mooring systems have been developed to mitigate the risks associated with the conventional mooring system, the majority of vessels continue to use ropes, fenders, and winches that allow berthing at most terminals. Therefore, it is still important to investigate the response of ships moored with the conventional system under various wave conditions.

2.3. Methods for estimating ship response in ports

A reduction in wave heights does not necessarily imply the same reduction in the moored ship response (López and Iglesias, 2014; Van der Molen et al., 2016). As a result, evaluating the moored ship behaviour at terminals in waves needs a detailed investigation of not only wave heights at the berthing site but also wave period and direction, wind, current, water depth, berthing structure features and the characteristics of moored body and mooring system. The combined interaction between those variables can be adequately described by solving the hydrodynamic problem including a dynamic mooring analysis. To account for all these variables in numerical simulations, the

numerical models must be rather complicated. On the other hand, physical model testing or full-scale measurements for ship motions, fenders and mooring line configurations help to validate the numerical models and understand the complex ship behaviour at a specific berth site under severe dynamic actions.

A basic static mooring analysis can be employed only when the variations in wind and current forces are slow enough for the mooring system to respond in a quasi-static way (OCIMF, 2018). Therefore, the appropriate modelling approach for the dynamic problem is determined by the features of the location and what is being studied.

2.3.1. Numerical models

Some numerical models estimate responses based only on local wave data. Van Oortmerssen (1976) developed a frequency-domain numerical model based on the Boundary Element Method (BEM) to predict the dynamic behaviour of a moored tanker near the quay wall in irregular waves. Xiong et al. (2015) used the SESAM software to assess the response of a moored barge in shallow open water. Abdelwahab et al. (2021) applied the time-domain software AQWA to estimate motions and loads in long-crested waves at a constant depth, including nonlinear mooring. Ma and Yan (2009) introduced a quasi-arbitrary Lagrangian-Eulerian finite element model (QALE-FEM) based on non-linear potential theory to simulate responses of moored floating bodies to steep waves.

Other advanced hybrid numerical models (Bingham, 2000; De Bont et al., 2010; Pinheiro et al., 2015; Van der Molen, 2006; Van der Molen et al., 2016; Van der Molen and Wenneker, 2008; Wenneker et al., 2006) account for the nonlinear impacts of wave propagation from an offshore point, harbour geometry, berth bathymetry, and mooring characteristics. In these numerical models, the nearshore wave transformation effects were captured using Boussinesq-type wave propagation models. Then, the hydrodynamic coefficients and wave exciting forces on the moored ship were calculated using three-dimensional diffraction models. Finally, the motions in the six degrees of freedom (6-DOF) are obtained by solving the equations of motions in the time domain as proposed by Cummins (1962), including nonlinear viscous damping and mooring effects.

Recently, numerical models have become more accurate. Dobrochinski (2014) and Dobrochinski et al. (2023) estimated moored ship responses using the open-source non-hydrostatic wave-flow model SWASH presented by Zijlema et al. (2011) instead of applying Boussinesq-type wave propagation models. To analyse the motion of moored ships in port under resonance conditions, Kumar et al. (2016) integrated a 3D BEM frequency domain model in the moored ship area with a linear 2D BEM model that solves the Helmholtz equation in a harbour. Kwak and Pyun (2013) and Kwak (2018) combined a 2D finite element wave model (CGWAVE), based on the elliptic mild-slope wave equations, with a three-dimensional Green's function model to predict moored ship motion considering harbour resonance.

The above-mentioned coupled wave-panel models are limited to weakly nonlinear wave conditions. Therefore, Rijnsdorp and Zijlema et al. (2016) extended the SWASH model to tackle the wave diffraction problem for non-moving floating bodies taking into account the nonlinear transformation of waves and shallow water flows over complex bottom topography in coastal regions up to the shore or harbour. Rijnsdorp et al. (2022) further extended the model to capture the wave-structure interactions and the wave-induced response of a moored ship in coastal waters. However, the poor schematisation of floating bodies prevents the inclusion of sophisticated hull details like a bulbous bow.

2.3.2. Field observations and physical model testing

Due to the complexity of the hydrodynamic problem involved in the dynamic mooring analysis in the form of viscous effects, turbulence, and high-order interactions, most advanced numerical models may still have limitations (Rosa-Santos and Taveira-Pinto, 2013). Consequently, numerical simulations should still be calibrated and validated with full-scale field data, physical model measurements, or benchmark solutions such as analytical or other numerical models. Furthermore, the efficacy of novel mooring systems and their proper representation in numerical models can only be verified by full-scale or model-scale measurements (De Bont et al., 2010; Kim et al., 2014; Van Deyzen et al., 2015; Yoneyama et al., 2004).

Field observations for ship motions and mooring loads at terminals are often limited, and the majority of the available data comes from port operator observations (Kwak and Pyun, 2013; Sakakibara and Kubo, 2008a) or small field campaigns (Figuero et al., 2019; Kubo et al., 2001; López and Iglesias, 2014; Uzaki et al., 2010; Van der Molen, 2006). It is also worth noting that measuring loads on lines and fenders at full scale is more challenging than measuring motions. Taveira-Pinto et al. (2008) proposed a methodology that combines numerical models, physical modelling and field measurements to estimate the responses of moored ships and loads in ports. Recently, Costas et al. (2022) presented an integrated method for evaluating basin-vessel resonance by combining full-scale data with numerical modelling.

Physical model testing is a useful technique for studying the behaviour of moored ships at berthing facilities inside ports or offshore terminals, under various combinations of design parameters and complex environmental conditions. Scales ranging from 1:75 to 1:150 were recommended by Hughes (1993) to study the moored ship behaviour in a harbour. The American Society of Civil Engineers recommended physical model studies to test and develop the mooring system in areas with significant dynamic actions on the vessel (ASCE, 2014). The opportunity to test various scenarios in the tests aids in achieving optimum operating conditions at the berth Taveira-Pinto et al. (2008). Weiler et al. (2009) used a combination of a time-domain numerical model with physical models to study the effect of gusting wind on an LNG carrier moored at an open jetty. Rosa-Santos et al. (2014) assessed the combined effects of mooring pretensions and ship-fender friction forces on moored ship responses, using a 3D physical model at a scale of 1:100, to enhance operational and security conditions at a berthing site. Baker et al. (2016) applied large-scale physical models to assess and optimize the preliminary design for a new container terminal, as well as to predict the operation downtime at various terminal layouts and configurations. Demenet et al. (2018) proposed a physical model study to evaluate the effect of various harbour structure configurations on the behaviour of moored ships at different water depths, wave conditions, and wave directions. Esferra et al. (2018) studied several mooring configurations at a port terminal using physical modelling to ensure safe mooring under significant tidal current effects. Dong et al. (2022) experimentally investigated the moored ship response at low frequency harbour oscillations. Based on experimental model testing, this paper investigates the behaviour of a moored ship at the port of Leixões, including a major modification in the north breakwater.

2.4. Safe operation criteria

Depending on the type of vessel and the direction of the waves, the Spanish standards ROM 2.0–11 (Puertos del Estado, 2011) established significant wave height constraints for safe loading and unloading operations at berthing sites. In addition, López and Iglesias (2014) advocated for establishing a new threshold at the berthing site for wave energy in the low-frequency band to guarantee safe operational conditions for moored vessels. OCDI (2020) established guidelines outlining the maximum allowable significant wave heights for cargo handling operations at long wave periods. These limits are determined based on either the size of the ship or the surge resonant period.

The primary function of a ship mooring system is to ensure not only safe mooring but also cost-effective and efficient cargo handling operations. The reduction of the motions does not necessarily give a similar reduction of downtime (Van Deyzen et al., 2014). While each mooring configuration is unique, the relevant criteria for safe and efficient

mooring should be addressed during the downtime assessment. Both ship motions and mooring loads on each mooring element are the essential design factors for satisfying operational and safety criteria at berthing structures (Taveira-Pinto et al., 2008). For example, moored tankers are limited by 3 m in surge motion and 4 m in sway to avoid damage to the loading arm and cargo manifolds. Likewise, ramp and crane operations severely limit the allowable motions of RO-RO vessels and container ships, respectively (Elzinga et al., 1992; PIANC, 1995; Van der Molen, 2006).

OCIMF (2018) specified the maximum load that a mooring line should be subjected to in both ship design and operational service as 55% for a steel wire or 50% for a synthetic rope of the ship design minimum breaking load (MBL) of a mooring system that is designed to fulfil the OCIMF standard environmental criteria. Also, the maximum allowable reaction of the installed fenders may not be exceeded. Lee et al. (2021) presented novel numerical simulations to evaluate operation efficiency based not only on criteria for ship motions, fender forces, and mooring line tensions but also on mooring line temperature caused by internal and external frictions and bending fatigues. Other factors, such as terminal operator skills, may also have an impact on operability (Molina-Sanchez et al., 2020). However, the development of the safety criteria and their relationship to operability remain uncertain. The aforementioned thresholds for wave heights, motions and loads are international standards that can be applied to various berthing facilities. Due to the lack of site-specific criteria for the port of Leixões in the literature, they are implemented in this paper to evaluate the operability through a mono-parametric downtime assessment at various sea conditions and mooring configurations.

3. Experimental study

3.1. Study area: Leixões oil terminal

The port of Leixões is one of the largest ports in Portugal (Santos and Guedes Soares, 2017), which is located 9 km northwest of the city of Porto as shown in Fig. 1(a and b). The port is accessed by different types of ships that approach it from different routes that can be seen in the data from the Automatic Identification System, which also allow the identification of the trajectories to different terminals of the port (Liu et al., 2023). The port is protected by two curved breakwaters that enable the reception of around 2700 ships of various types per year (APDL, 2016). It has an oil terminal with three berth sites (A, B and C) as shown in Figs. 1(c) and 2. The latter two are sheltered inside the port area in shallow water, while berth (A) is located behind the north breakwater near the port's entrance to accommodate large oil tankers at a loading platform with two breasting dolphins and floating pneumatic fenders. Therefore, berth (A) is frequently exposed to severe waves that reach the Portuguese coast from directions between west and northwest (Capitão et al., 2017; Lucas et al., 2023; Rosa-Santos et al., 2008; Rusu and Guedes Soares, 2011), resulting in a significant wave height of 2.5 m near it. Studies showed that wave overtopping, wave diffraction, current and sediment transmission, longwave impacts, and mooring configurations contribute to adverse wave conditions and berth operability (Veloso-Gomes et al., 2005).

A single-point mooring buoy was placed offshore to preserve the cargo handling operations of large oil tankers during poor weather conditions. Rosa-Santos et al. (2008) and Rosa-Santos and Taveira-Pinto (2013) suggested countermeasures to reduce the downtime at the Leixões oil terminal, such as optimizing the cross-section of the current breakwater structure to reduce overtopping and enhance the stability of the armour layer. Additionally, they recommended modifications to the mooring setup, pretensions, water depth, and local interventions at the head of the existing north breakwater, such as extending the existing upright wall or constructing a roundhead wave-breaking bank. Recently, the average size of the ships that demand Leixões port increased by 77% (APDL, 2016). Therefore, the Leixões port authority APDL approved extensive modifications to the port layout to increase the shelter condition and allow larger ships access. The outer north breakwater will be extended by 300 m with a 20° opening angle relative to the existing breakwater. Furthermore, the entrance channel and turning basin will be dredged to a deeper water depth as shown in Figs. 1(c) and 2.

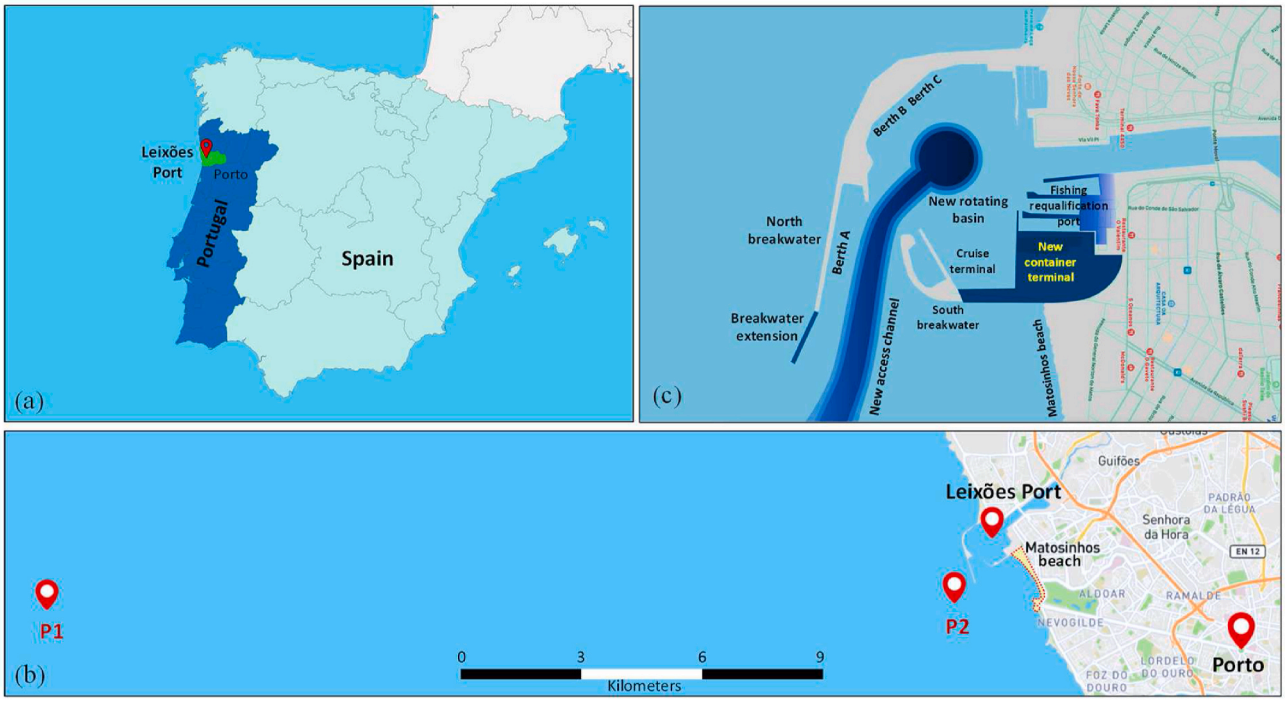

Fig. 1. (a) Iberian Peninsula showing Leixões port, (b) Location of the port of Leixões, Matosinhos beach and two evaluation locations (P1 and P2) for wave condition, and (c) General layout of the port of Leixões (APDL, 2022).

Fig. 2. Modifications to the layout of the port of Leixões as reconstructed from APDL (2016).

3.2. Testing facility and model layout

The physical model experiments were performed at the wave tank of the Maritime Hydraulics Experimental Unit (UEHM) in the Department of Hydraulics and Environment (DHA) of the Portuguese National Laboratory for Civil Engineering (LNEC) as shown in Fig. 3. The testing tank is 44 m long and 23 m wide. Waves were generated with a 6 m wide mobile piston paddle wave generator, which is powered by a hydraulic jack to produce unidirectional regular and irregular waves at a water depth of up to 0.5 m. Portable water barriers were used to direct the generated waves towards the port in the physical model.

Testing physical models on different scales is ideal for mitigating scale-related influences on results. However, budget and time limitations may lead to choosing a model scale similar to prior studies. In this study, the Froude scaling was applied in compliance with the experimental tank size to construct a three-dimensional model of the entire new basin of the port of Leixões at a scale of 1:80 as shown in Fig. 3, which is suitable for this type of study as recommended by Hughes (1993), as it ensures accurate inertial-to-gravitational force representation. The model incorporates the modified port configuration as well as the new sea bed bathymetry −16.85 m from the zero hydrographic level (ZHL) for the entry channel and −15.5 m (ZHL) for the turning basin as specified by APDL (2016). It also includes the adjacent beach of Matosinhos, the existing south and north breakwaters and mortar surface reproducing the seabed bathymetry up to −20 m (ZHL) at which the wave generator is settled in the tank.

A 300 m extension of the north breakwater with an opening angle of 20° relative to the alignment of the existing breakwater was constructed in the physical model to investigate the future upgrade approved by APDL (2016). To provide realistic wave conditions near berth (A), all sheltering structures were replicated in the physical model. Furthermore, a dissipative absorbing wave beach was built along the basin's boundary to reduce the reflections. Fig. 4 shows a sketch of the physical model of the port of Leixões in LNEC's wave basin. The coordinate systems adapted in the study are the basin-fixed reference frame and the moored ship local reference system.

Scale effects may have a notable influence on the stability of the armour blocks used to replicate the new extended sheltering structure and on the transmission phenomena. To assess and optimize the design of the extended breakwater, additional physical models of the new extension have been thoroughly investigated in the experimental facilities of LNEC at larger scales (Fortes et al., 2017). Two alternative cross-sections for the trunk of the new extended rubble-mound breakwater were tested at different sea states and tidal levels, by two-dimensional physical models at a scale of 1:61 in a flume at LNEC (Lemos et al., 2017a). In addition, a larger three-dimensional physical model, scaled at 1:63, was constructed to examine the stability of blocks in the armour layer and wave overtopping events at the new breakwater extension under various testing conditions (Lemos et al., 2017b). This larger 3D model solely replicated the head and trunk of the future 300 m north breakwater extension, including the bathymetry up to approximately 50 m of the existing breakwater. This approach allowed for

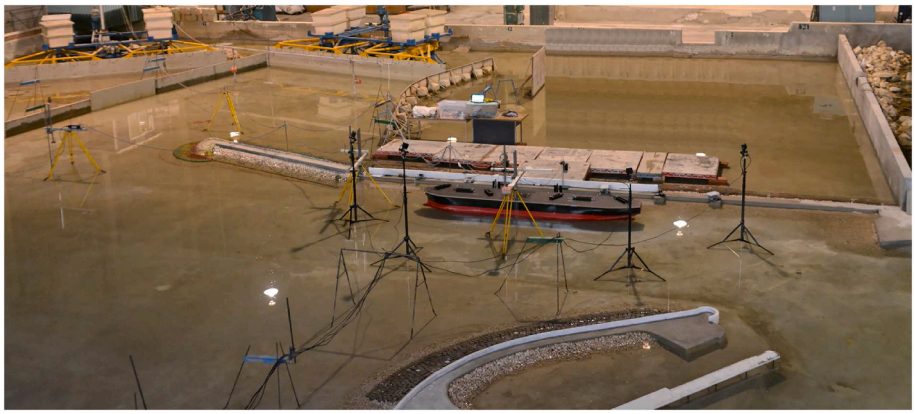

Fig. 3. The physical model of Leixões port at LNEC's wave basin.

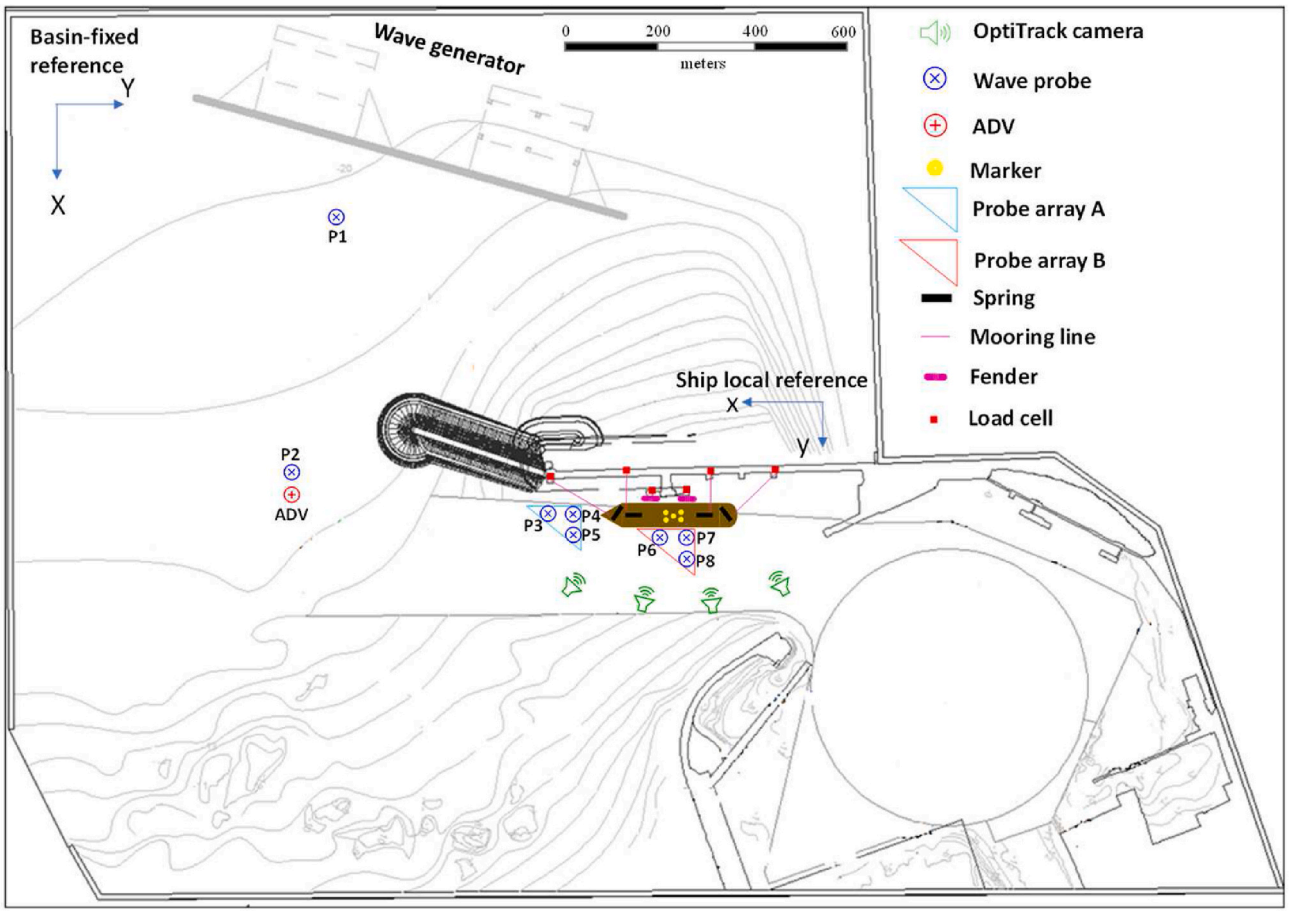

Fig. 4. Sketch of the physical model layout in LNEC's wave basin.

accurate wave diffraction modelling around the head of the breakwater extension while minimizing construction work and associated costs by excluding the remaining portion of the breakwater structure. Furthermore, several numerical studies were carried out to investigate multiple alternatives for the configuration of the new extended breakwater (Fortes et al., 2017).

Part of the numerical studies focused on the estimation of wave conditions at the entrance of the port of Leixões (P2) based on data from offshore points such as (P1) (Capitão et al., 2017; Rusu and Guedes Soares, 2011), as well as the influence of various climate scenarios on the harbour resonance and wave propagation inside the port (Pinheiro et al., 2017a, 2017b) and to the nearby Matosinhos' beach (Pinheiro et al., 2017c), as shown in Fig. 1(b). The other numerical studies concentrated on the impact of the new extension on the dynamic sediments inside the port and the beach of Matosinhos (Fortunato et al., 2017a, 2017b).

This paper focuses solely on the 1:80 scale 3D model of the whole basin of the port of Leixões. The entire test programme was conducted considering multiple testing parameters: tide level, mooring system pretension, and sea state severity condition (Hs and Tp). Santos et al. (2019), Pinheiro et al. (2020b, 2020a) and Abdelwahab et al. (2021) reported some test campaign results. Furthermore, Abdelwahab and Guedes Soares (2023) thoroughly evaluated the experimental uncertainty in the physical model and measured data. The goal of this paper is to analyse the influence of sea severity and mooring pretension configurations on both wave conditions at berth (A) and the operability of the Osaka tanker moored at the berth in terms of motions and mooring loads, considering the APDL's approved future modifications in the layout of the port of Leixões.

3.3. Experimental equipment

A ship model and three primary measuring systems were employed in the physical model study. The first is a wave measuring system, followed by a custom-designed mooring system, and the last is the motion capture system. To get an accurate measurement under the various testing parameters, the operation of the equipment and systems is maintained as illustrated in Fig. 5. Before testing in waves, the calm water condition in the tank is confirmed to avoid tank disturbances effects on the measured data. The procedure begins with data acquisition systems collecting data for waves and mooring loads while concurrently tracking target markers onboard the moored model using the motion capture system. The synchronisation of the three systems is therefore assured.

3.3.1. Ship model

The Very Large Crude Carrier (VLCC) Esso Osaka is selected in this study to investigate the motions and mooring loads. The model resembles the large ships that operate at berth (A) in the port of Leixões. In addition to the geographic and bathymetric aspects of the area included in the model, the Esso Osaka ship is also replicated at a scale of 1:80, adhering to Froude similarity. The hull of the ship model is made of fibreglass-reinforced plastic. The hull was covered with an 18 mm hardwood deck for the present study to aid in the installation of mooring equipment and motion target markers.

As the displacement of the ship affects the natural period of the dynamic moored system, the ship model is calibrated in calm water, before being tested in waves, to obtain the main model characteristics listed in Table 1. To replicate the required displacement weight at an even keel draft T = 0.132 m at the model scale, concrete ballasting weights were

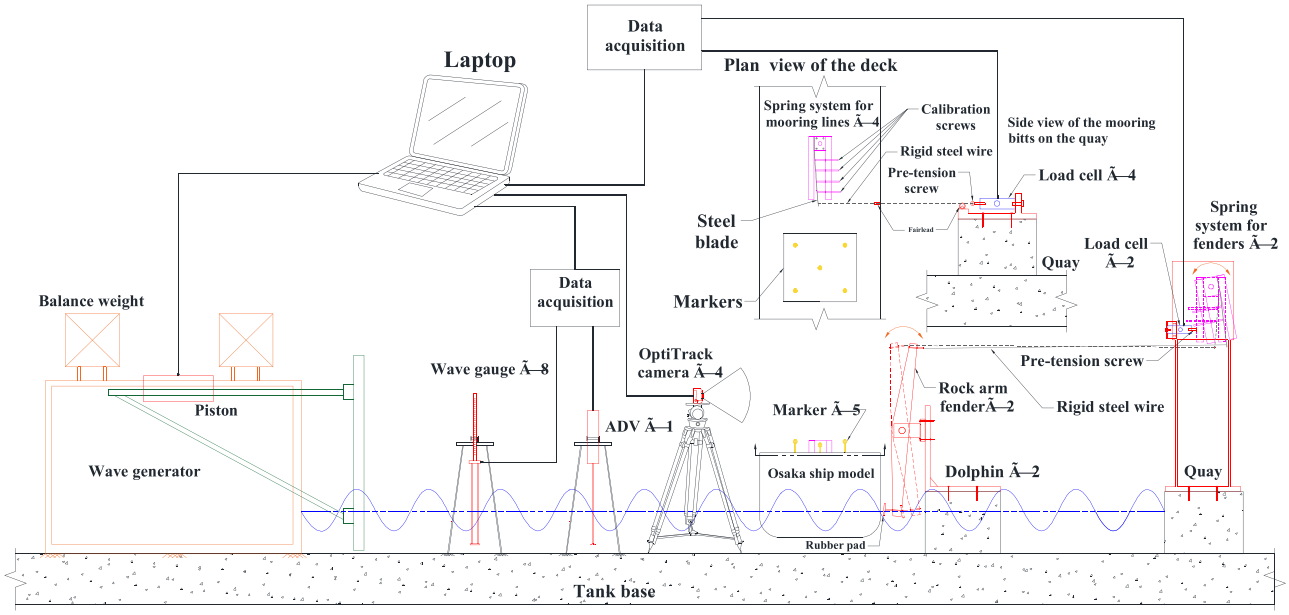

Fig. 5. Experimental equipment involved in the physical model.

Table 1
Main characteristics of the free-floating Esso Osaka ship in model scale.

Parameter	Symbol	Units	Value (model scale)
Length between perpendiculars	L_{pp}	m	3.2500
Beam	B	m	0.5300
Depth	D	m	0.3470
Draft	T	m	0.1315
Displacement	Δ	kg	186.8040
Block coefficient	C_B	–	0.8240
Mid-ship section coefficient	C_M	–	0.9970
Waterplane area coefficient	C_{WP}	–	0.8520
Longitudinal centre of gravity (fwd+)	LCG	m	0.2351
Metacentric radius	BM_T	m	0.1656
Metacentric height	GM_T	m	0.0779
Vertical centre of gravity	KG	m	0.1551
Roll natural period	T_n	s	1.5321
Linear roll damping factor	ζ	–	0.0228
Roll radius of gyration	K_{xx}	m	0.1850
Pitch radius of gyration	K_{yy}	m	0.8120
Scale factor	-	–	1:80

distributed within the ship model. The vertical centre of gravity KG and metacentric height GM_T were then determined using inclining experiments. After that, six free decay tests for the free-floating model were conducted to determine its roll natural period and damping ratio. Significant damping in heave and pitch motions made it challenging to ascertain their natural periods through decay tests.

3.3.2. *Wave measurement system*

The wave measurement system consisted of eight resistive wave probes (HR Wallingford) and one (Vectrino) down-looking Acoustic Doppler Velocimeter (ADV), which were arranged to assess wave conditions at four distinct sites around the basin as shown in Fig. 4. A wave probe (1) was placed in front of the wavemaker to assess the incident wave condition, while a second wave probe (2) was paired with ADV to study the wave elevation and direction at the port entry. The directional wave spectra around the moored model were evaluated using two probe arrays made of three probes each. The probes in each array made a triangle whose side length is approximately 5–10% of the dominant wavelength. Array (A) combines wave probes (3, 4, and 5) in front of the moored ship, whereas array (B) combines probes (6, 7, and 8) beside the moored ship's centre of gravity. The signals collected by the various wave probes and the ADV were synchronized at a sampling frequency of 25 Hz.

3.3.3. *Mooring system*

It is crucial to replicate the real mooring system in scaled physical models for moored ships using scaled mooring equipment, often referred to as 'simulators'. These simulators must be capable of measuring the forces acting on the mooring system while simultaneously simulating the characteristics of the lines and fenders in the model scale. At LNEC's workshop, novel custom-designed mooring simulators were manufactured to replicate a generic asymmetric nonlinear mooring configuration of four mooring lines and two fenders, as illustrated in Fig. 6. The mooring points were chosen in the tank based on the precise placements of the mooring bitts on the quay as shown in Fig. 7. The real scale characteristics of the mooring system at berth (A) in the port of Leixões are described by Rosa-Santos and Taveira-Pinto (2013). However, owing to the limited available equipment during testing, fewer lines are employed in the presented physical model to depict a similar asymmetric starboard mooring configuration.

Six load cells of the tension-compression S-type with an accuracy of ±0.03% were employed to quantify the loads on the mooring lines and fenders at 50 Hz, as shown in Figs. 5 and 7. The maximum capacity of each load cell is 2 kgf at the model scale. Two rocking arm fender simulators with rubber pads were utilized in the experiments to replicate the behaviour of the fenders, simulate the ship-fender friction interface, and record the compressive loads imposed on the fenders by the moored model. Four mooring line simulators were used to model the stiffness of real mooring lines and measure the tension loads on the mooring lines. All simulators were equipped with nonlinear cantilever spring systems and pretension screws. In addition, frictionless fairleads were placed on the wooden deck and quay to direct the inelastic mooring steel wires to the connection points as shown in Figs. 5 and 7. The spring systems proposed by Marcos-Rita (1984) were used to model the non-linear elastic characteristics of the lines and fenders. Additional details for these spring systems are explained in (Abdelwahab and Guedes Soares, 2023). The specified load-elongation or deflection curves are used to define the length of the leaf springs (L), as well as the number and spacing (S_i) of the adjustment screws shown in Fig. 8(a) and (b). To achieve the requisite scaled model stiffness of each mooring element, several calibration weights were hung from the free end of each leaf spring to properly estimate the calibration screws' length (Z_i) in each

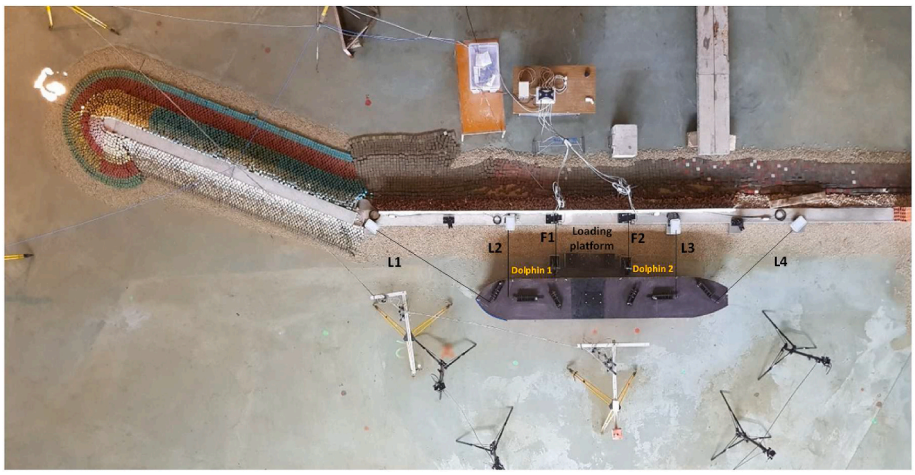

Fig. 6. The mooring arrangement in the physical model.

Fig. 7. Physical model of fenders and mooring lines.

spring system. Fig. 8(c) shows examples of the calibrated load stiffness for mooring lines and fenders.

Various mooring concepts can be employed to simulate moored systems with physical models. Some of these concepts, such as those developed by Cornett et al. (2012), Esferra et al. (2018), Rosa-Santos et al. (2014, 2010) and Rosa-Santos and Taveira-Pinto (2013), have employed different techniques involving coiled springs, inelastic fibre strands, pretension weights, pulleys, and Linear Variable Differential Transformers (LVDT) or cantilever force transducers, to replicate aspects of mooring lines and fenders. However, these existing mooring simulators are limited to reproducing only linear and bilinear load-deformation behaviour for mooring lines and fenders, respectively. They fall short of replicating the actual nonlinear load-deformation relationship observed in real prototypes. In contrast, the novel custom-made mooring system simulators, featured in this study, accurately replicates various nonlinear load-deformation relationships, as depicted in Fig. 8. This is achieved by simply adjusting the length of screws and leaf springs. The full-scale nonlinear properties of a real mooring system can be replicated by combining nylon lines and elastic steel sheets, connected to load cells, and by utilizing a special fender gauge as presented by Dong et al. (2022). This approach yields nonlinear load-deformation relationships; however, it requires expensive equipment, with a market price of 29,700 EUR, to simulate 2 fenders and 4 mooring lines in a physical model. In contrast, the novel custom-made mooring system simulators utilized in this study are primarily constructed from acrylic material, steel leaf springs, screws, roller bearings, and steel wires, with a fabrication cost of 750 EUR for a set of 6 simulators. They are connected to standard force transducers, which have a market price of 3500 EUR for a set of 6 load cells. Therefore, the presented custom-made simulators may replicate accurate full-scale characteristics and offer a cost-effective alternative to expensive mooring equipment typically employed in most testing laboratories to physically model a real mooring system.

3.3.4. Motion capture system

The OptiTrack™ motion capture system was used to measure the response of the Esso Osaka model. The system has the benefit of recording the motions without coming into contact with the model. It is made up of four digital cameras that recorded the moored model's motions in 6 DOF using multiple markers mounted on its deck, as illustrated in Fig. 5. The markers' movements were then transferred to the centre of gravity, from which a time series of ship motions were measured at a sampling frequency of 120 Hz. The cameras have a three-dimensional accuracy of ±0.2 mm for translational motions and ±0.01° for rotational motions.

3.4. Testing procedure and conditions

The impact of sea severity on the wave condition at the modified berthing site, as well as motions and mooring loads at various pretension configurations, were examined experimentally under all possible combinations of the testing conditions illustrated in Table 2. Before the start of the wave tests, the ship model was centred and moored, against the two breasting dolphins and the loading platform at berth (A) as shown in Fig. 7, using the nonlinear mooring configuration described in section 3.3.3. Then, all measuring equipment and the calm water level were calibrated, and the equipment's zero levels were confirmed.

In practice, all mooring lines must be kept taut to ensure that the mooring system is always active. As a result, the target pretensions are applied in mooring elements by adjusting the pretension screws linked to the load cells to shorten or extend the wires. Two distinct pretension configurations are used in this study. First, a low pretension configuration with loads rated at 110–250 kN in full scale. Second, a high pretension configuration with a range of 300–600 kN is used as shown in Table 2. A friction coefficient of 0.33 was predicted based on a static friction experiment for a wet interface between fibreglass and rubber pads.

Again, decay tests were conducted with the ship moored in calm waters to estimate the natural periods. A force was applied to induce displacement or rotation from the ship's equilibrium position. Subsequently, these forces were abruptly removed, causing the ship to oscillate around its equilibrium. Fig. 9 shows the recorded signals during the decay tests for the moored and free-floating models. Table 3 shows the estimated damping ratios and natural periods of the moored ship in model scale at different pretension configurations. The analysis of the

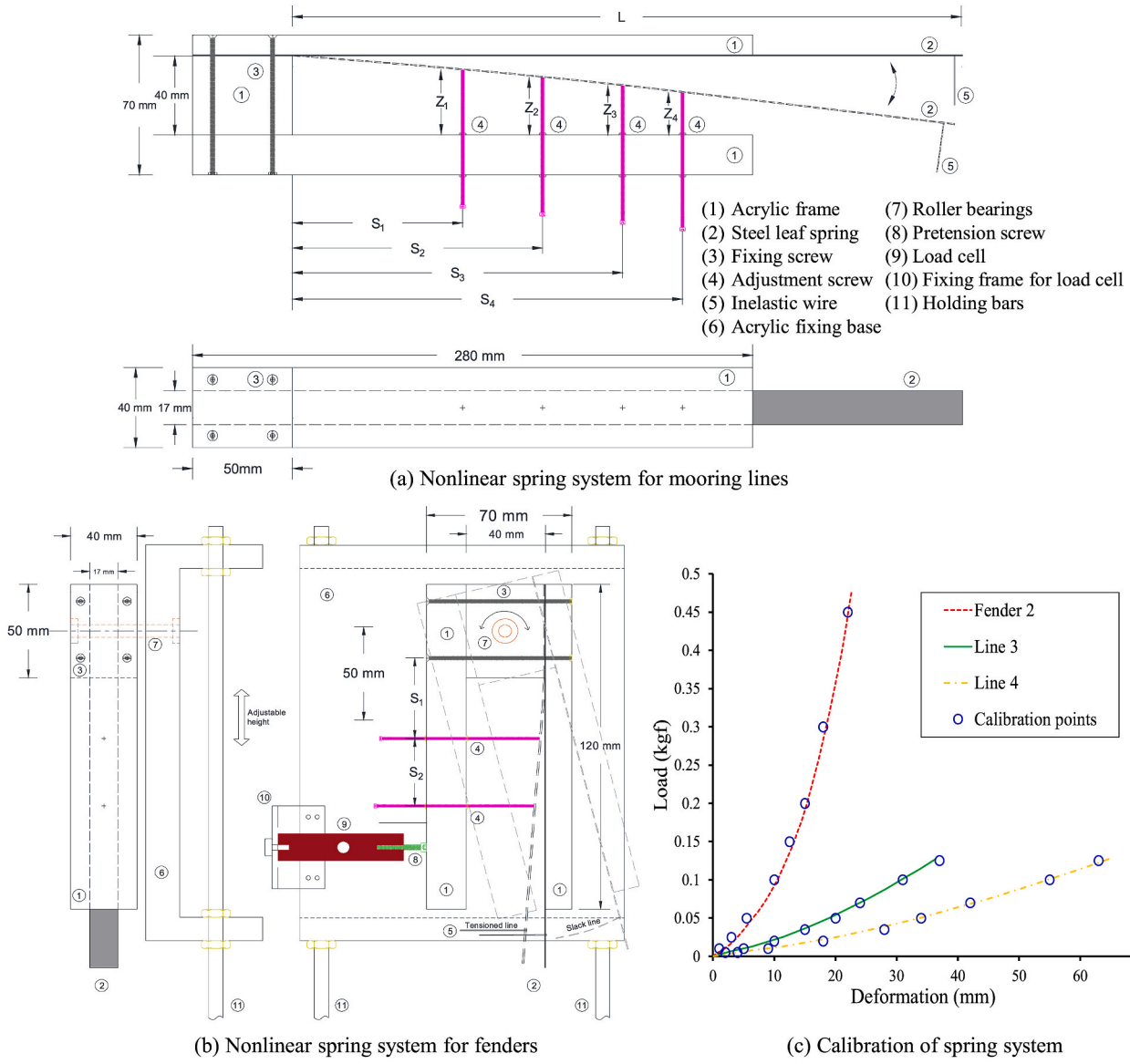

Fig. 8. Calibrated nonlinear mooring system in model scale.

Table 2
Testing conditions in full scale.

Parameter	Symbol	Unit	Value (real scale)	Comment
Pretensions	T_{low} T_{high}	kN	110–240 300–600	Range of loads in mooring lines and fenders
Significant wave height	H_s	m	3 4 6	Generated at the wavemaker positioned at −20 m (ZHL) following the analysis of data
Peak period	T_p	s	10 14 16	predicted by wave propagation models
Wave direction	θ	°	270	
Bathymetric level	z	m	−16.85	Measured at the berth location in the entry channel from the ZHL
Height of tide	HAT	m	+4	High tide measured from the ZHL
Depth	h	m	20.85	Water depth near berth A
Friction	μ	–	0.33	Rubber material

results shows that the natural periods of the moored ship's horizontal plane motions are relatively long, and they vary depending on the type of pretension utilized. On the other hand, the roll natural period is less affected by changes in pretensions.

The moored Esso Osaka tanker model should start each test at the same equilibrium position to ensure that the results achieved under multiple incident wave scenarios are comparable. As a result, the pretensions were recorded shortly before the tests began and after the tests were complete. Table 4 gives an example of a comparison of mooring element pretensions before and after the tests. The negative load indicates the fender's compression force, whereas the positive load represents mooring line tension.

The tested wave parameters (H_s, T_p and θ) were selected after a detailed analysis of the wave condition shown in Table 5 at a local point P2 (41° 10′ 5.7″ N, 8° 42′ 51.59″ W) in the vicinity of the future extended north breakwater of the port of Leixões at a bathymetric level of approximately −20 m (ZHL) as shown in Fig. 1(b). This local wave condition was predicted based on numerical simulations of a wave propagation model (SWAN) that utilized as boundary conditions the wave data from a hindcast model (WAM) forced by wind fields provided by the European Centre for Medium-Range Weather Forecasts (ECMWF)

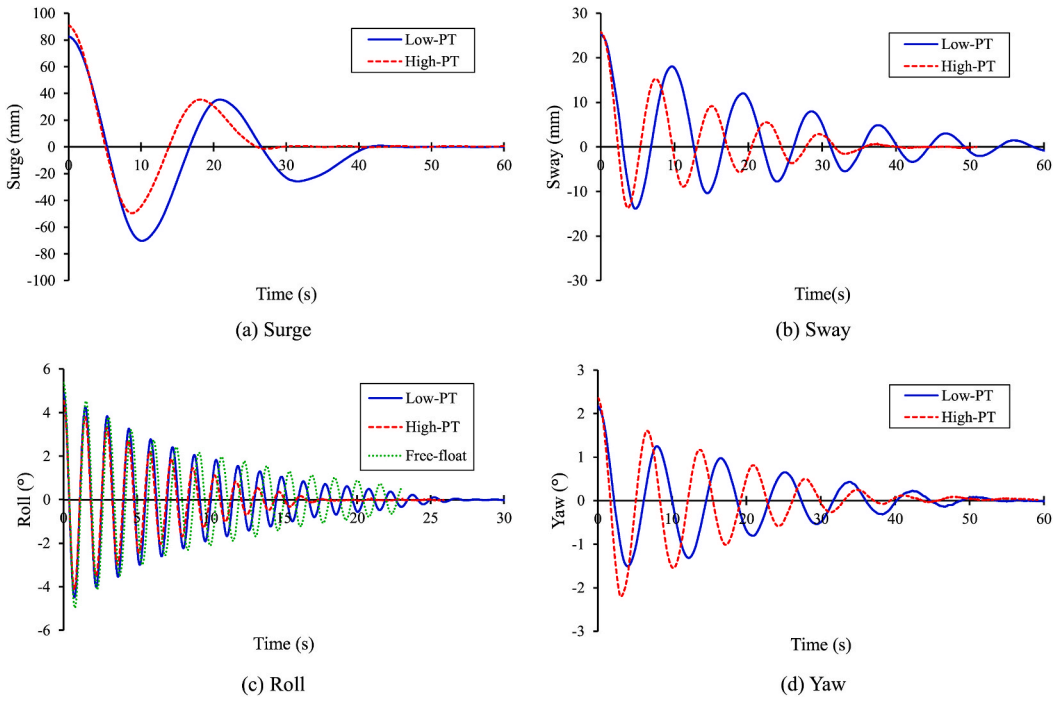

Fig. 9. Time series of the decay tests of the moored Esso Osaka model.

Table 3
Natural periods of the moored ship in model scale.

Motions	Natural period (s)		Damping factor	
	Low-PT	High-PT	Low-PT	High-PT
Surge	19.3	17.9	0.163	0.168
Sway	9.13	7.43	0.069	0.086
Roll	1.48	1.46	0.024	0.035
Yaw	8.43	6.84	0.071	0.064

Table 4
Example of the recorded pretensions on mooring elements before and after testing in model scale.

Mooring element	Length (m)	Low pretension (N)		High pretension (N)	
		Before	After	Before	After
Bowline L1	1.9	0.4467	0.4435	0.6058	0.6233
Breast bowline L2	0.95	0.2321	0.2277	0.7388	0.7093
Forward fender F1	–	−0.4587	−0.4511	−1.1310	−1.1419
Aft fender F2	–	−0.4576	−0.4653	−1.1746	−1.1158
Breast Stern line L3	0.87	0.2299	0.2201	0.7497	0.7616
Stern line L4	1.5	0.4413	0.4555	0.5808	0.5372

Table 5
Predicted wave data at point P2 near the future extended north breakwater.

Wave data	H_s (m)	T_p (s)	Direction (degree)
Average	3.58	8.7	295
Minimum	–	3.9	182
Maximum	8.98	17.3	342

for a period of 38 years at an offshore point P1 (41° 10′ 00″ N, 8° 59′ 00″ W) far from Leixões port (Capitão et al., 2017), as shown in Fig. 1(b). The description of the various hindcast studies that produced that type of data can be found in (Rusu et al., 2008; Guedes Soares et al., 2011; Rusu and Guedes Soares, 2011, 2013).

The wavemaker at the basin is utilized to create unidirectional irregular waves that follow a JONSWAP spectrum formulation. The long-crested waves are generated with a direction of 270° to travel perpendicular to the new breakwater extension, as illustrated in Fig. 4. Although mixed swell and wind waves (Guedes Soares, 1984) may appear at any port entrance, the physical model tests were conducted only under unidirectional irregular waves due to experimental facility restrictions. The target sea states at the wavemaker, located at point P2, are characterized by significant wave heights H_s ranging from 3 to 6 m and peak period T_p ranging from 10 to 16 s (real scale) as shown in Table 2.

The selected wave conditions were calibrated before starting the tests of the moored ship, to ensure a realistic environment for the modelled waves. The irregular wave signal comes from the wave generator as a sum of about 1000 wave components of different frequencies. Calibration has been conducted by comparing the characteristics of targeted sea states to the generated measurements at a predefined point near the wavemaker. A 5% acceptance criterion for both significant wave height and peak wave period was used. Fig. 10 shows examples of comparison between the target and measured wave spectra in front of the wave generator at sea states characterized by peak wave period of 14 s and at significant wave heights of 2, 4 and 6 m (real scale).

The experiments were carried out at low and high tide levels, with an approximate full-scale bathymetric level of −16.85 m (ZHL) at the entrance channel berth site. This paper presents only the results at the high tidal level of +4 m in the full scale (ZHL), which gives a total water depth of 20.85 m in the full scale. Each test lasted for 20 min, representing a vessel being exposed to about 3 h of a real-world storm. The time interval between test runs was 25 min to minimize the residual disturbance in the testing tank.

3.5. Data analysis

3.5.1. Time domain analysis

The zero-crossing technique and other statistical tools are used to analyse the entire time series of each recorded signal, which includes free-surface elevation at different probes, motions in 6 DOF and mooring loads. The statistical results include the mean (A_m), skewness, kurtosis, and zero-peak amplitudes such as the maximum (A_{max}) and absolute

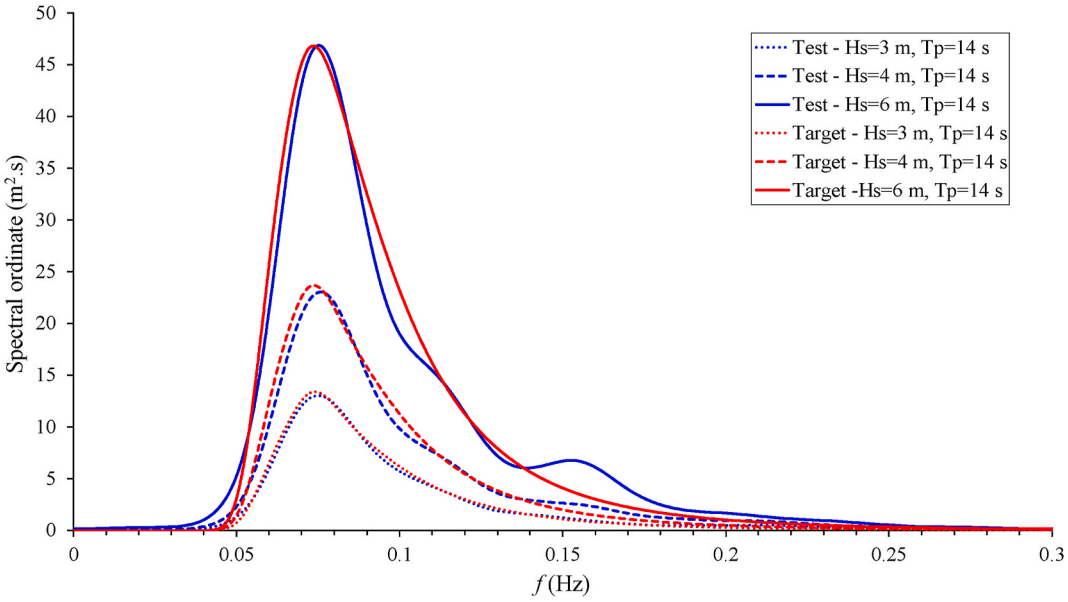

Fig. 10. Examples of the tested and target wave spectrum at wave probe P1 for different sea states.

minimum amplitude ($A_{\min}$) of each measurement. In addition, a peak-to-peak definition is applied to the entire time series of each signal to obtain the average peak-to-peak amplitudes (Z_{avg}), as well as the maximum peak-to-peak amplitudes (Z_{max}). The significant peak-to-peak amplitudes ($Z_{1/3}$) are evaluated as the average of the highest third peaks of each signal empirically. Finally, the obtained zero-peak and peak-to-peak amplitudes for motions are compared with the maximum values of the safe working limits prescribed by PIANC (1995) and Van der Molen et al. (2006). Likewise, the zero-peak amplitudes for loads are compared with safe working loads defined by OCIMF (2018).

3.5.2. Spectrum analysis

In addition to the time domain analysis, the frequency domain spectrum analysis is applied to produce energy spectra for waves, motions in the 6 DOF, and mooring loads from the entire time series of each recorded signal. The direct technique of Welch is applied in this paper to generate the power spectrum, in which the recorded signal is segmented into several sub-records with 50% overlap and filtered with a Hanning window. The Fast Fourier Transform (FFT) is then applied to each sub-record to estimate its power spectrum. Finally, the energy power spectrum of the entire signal is calculated by averaging all estimated power spectra. A comparison of the shape of the predicted wave spectrum and the targeted spectrum reveals that 128 segments are suitable for smoothing the wave power spectrum (Abdelwahab and Guedes Soares, 2023).

The power spectrum for each recorded signal is characterized by spectral significant amplitude Z_s which can be linked to the energy power spectrum $Z_s = 4\sqrt{m_0}$, where m_0 is the area under the entire energy spectrum curve. The period associated with the highest spectral ordinate in the entire spectrum is also defined as the peak period T_p. Furthermore, a frequency band ranging from $f = 0$ Hz to $f = 0.04$ Hz is used to define the low-frequency (long wave period) zone of the spectrum, which is characterized by the peak period T_{pL} and spectral significant amplitude $Z_{sL} = 4\sqrt{m_{0L}}$ that are associated with this band, where m_{0L} is the area under the defined low-frequency band of the spectrum curve. Additionally, the ratio of the energy in the low-frequency band to the total energy of the spectrum is defined by $R_L = Z_{sL}^2/Z_s^2$, which provides insight into the most energetic zone in the spectrum and aids in establishing the relationship between frequency bands in waves, motions, and load spectra.

3.5.3. Operability analysis

In this study, operability or operational efficiency is defined by comparing two probabilities: the likelihood of an abrupt system stoppage when it exceeds a specific mono-parametric operational limit versus the likelihood of the regular, expected stoppage when the operation normally concludes. To measure operability at the Leixões oil terminal, the experimental data during loading/unloading and bunkering operations are examined under diverse testing circumstances. The recorded time series for motions or mooring loads are compared against zero-peak safe operation limits, as depicted in Fig. 11. The loading operation is deemed unsafe with a mooring hazard if the recorded value exceeds the safety criteria. The mono-parametric operative threshold specifies the number of stoppages (N) that might occur during the entire operation (S_T) and the duration of each stoppage (S_i). Consequently, the operational efficiency shall be defined based on independent analysis of motion and load data as follows:

$$\eta = \left(1 - \frac{\sum_{i=1}^{N} S_i}{S_T}\right) \times 100 \tag{1}$$

4. Results and discussion

In the first and second parts of this section, the study examines how the offshore sea severity affects, respectively, the wave conditions at berth (A) and the operability at the berth, after constructing the newly extended breakwater. In the third part, the study evaluates the operability of loading/unloading of a moored tanker in terms of motions and mooring loads under various pretension configurations.

4.1. Influence of sea severity on wave conditions at berthing site

The experiments were conducted at various sea states to assess the influence of sea severity on wave conditions at the oil terminal's berthing considering a 300 m extension in the north breakwater. The wave data were collected at eight different places throughout the port. Fig. 12(a) shows an example of a recorded signal at wave probe number 3. Table 6 illustrates full-scale wave characteristics at each wave probe for a tested sea condition, with a significant wave height $H_s = 6$ m and peak period $T_p = 14$ s. The estimates of the significant wave height and peak period outside the port are around 5.9 m and 13.9 s, respectively,

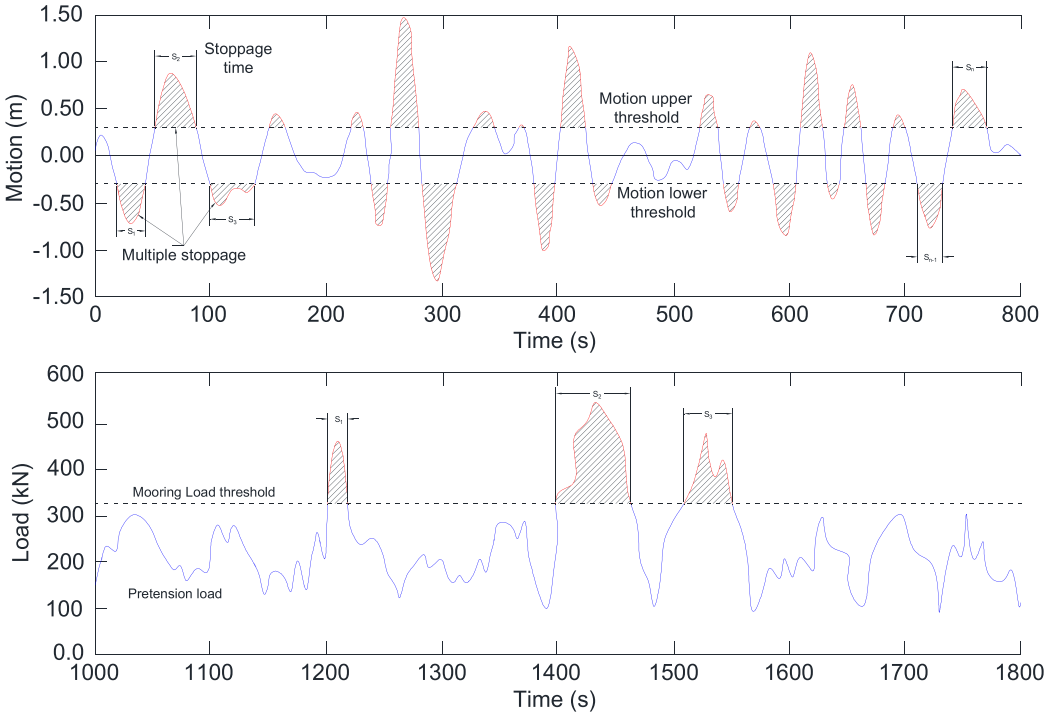

Fig. 11. Definition of efficiency based on mono-parametric operative thresholding.

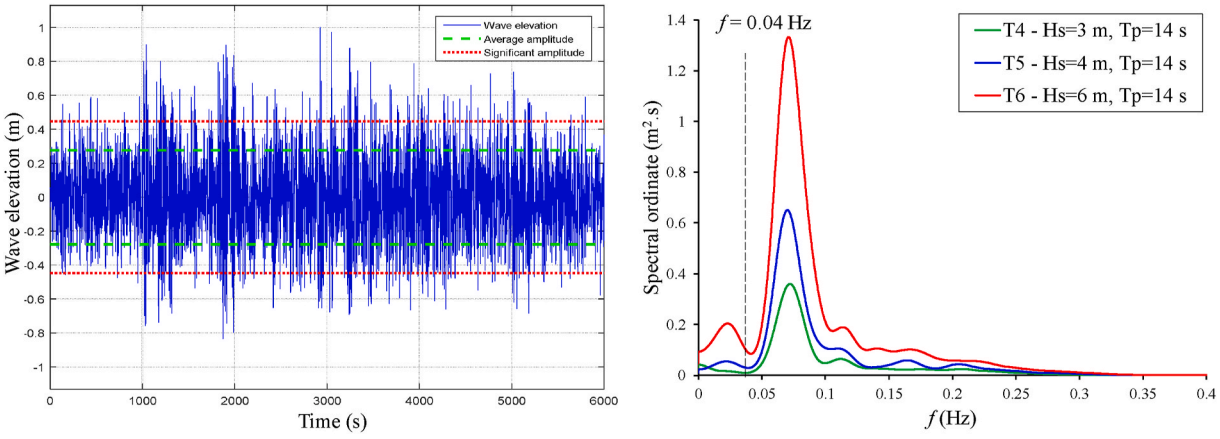

Fig. 12. Recorded wave data in full scale at probe 3 for $T_p = 14$ s and $H_s = 3$, 4, and 6 m.

Table 6
Wave characteristics at different probes for a sea state with $H_s = 6$ m and $T_p = 14$ s.

Analysis type	Wave properties	Units	Wave probes							
			P1	P2	P3	P4	P5	P6	P7	P8
Time domain parameters	A_{max}	m	6.301	2.947	1.076	1.127	1.116	0.831	1.015	0.952
	$A_{\min}$	m	4.359	2.577	0.833	0.950	0.950	0.858	1.011	1.022
	Skewness	–	0.304	0.226	0.139	0.148	0.120	0.161	0.152	0.172
	Kurtosis	–	2.933	2.916	3.199	3.164	3.098	2.762	2.803	2.826
	Z_{avg}	m	3.859	1.964	0.556	0.568	0.599	0.595	0.709	0.663
	Z_{max}	m	9.194	4.612	1.672	1.843	1.802	1.520	1.698	1.544
	$Z_{1/3}$	m	5.946	3.052	0.894	0.916	0.964	0.922	1.080	1.015
Welch spectral parameters	Z_s	m	6.120	3.211	0.979	0.996	1.033	0.961	1.143	1.067
	T_p	s	13.88	14.00	14.10	14.52	14.72	12.74	12.71	12.78
	Z_{sL}	m	0.459	0.288	0.306	0.290	0.281	0.214	0.250	0.246
	T_{pL}	s	26.28	26.83	40.24	40.24	40.24	80.49	80.49	80.49
	R_L	%	0.562	0.805	9.785	8.476	7.398	4.959	4.773	5.299

which match the targeted sea condition in that test. These values are also consistent with the spectrum analysis results. Results show that when the highest wave elevation outside the port reaches 6.3 m and the largest wave height is 9.2 m at wave probe number 1, the waves near the oil terminal's berthing site may have a maximum elevation close to 1.1 m and maximum wave height up to 1.8 m. When these values are compared to previous studies with the existing sheltering structure (Veloso-Gomes et al., 2005), the newly extended north breakwater shows a significant contribution to the reduction of maximum wave height at the berthing area at severe wave conditions.

Modified box-whiskers plots for the full-scale free-surface elevations acquired from the measured time series at all wave probes under various sea states are shown in Fig. 13, which may also provide information on the mean, maximum, minimum, and first and third quartiles. The experimental measurements acquired from wave probes placed close together exhibit comparable properties. The results demonstrate that the mean of all wave probe measurements is nearly zero. All wave probe measurements show low skewness. Furthermore, the kurtosis at all probes is close to 3, indicating that the probability density function of wave elevations may follow a normal distribution. In general, Fig. 13 shows that for all investigated sea states, the maximum and absolute minimum wave elevations increase as the tested significant wave height increases. They do, however, decrease as the waves travel to the berthing site.

Fig. 12(b) presents examples of wave spectra observed near the berthing site at wave probe 3 for sea states with a peak period $T_p = 14$ s and significant wave heights $H_s = 3$, 4, and 6 m, respectively. The results demonstrate that low frequencies up to 0.04 Hz have significant power spectra inside the port, which could indicate the presence of long-period waves at the berthing site near the bow of the moored oil tanker. Reflections from walls of the nearby structures or bathymetric effects may justify the existence of long waves.

Fig. 14(a) provides a comparison of significant wave heights acquired at all wave probes applying frequency domain analysis to the recorded data at various sea states. The results demonstrate that the measured significant wave height increases with wave severity, reaching 3.3 m at the port entrance (probe 2) and up to 1.2 m around the berthing site (probes 3–8).

Fig. 14(b) illustrates the progression of R_L, the ratio of energy in the low-frequency band to the total energy in the spectrum at various sea states across the port. In comparison to short waves, long waves outside the port (wave probe 1) and at the port entry (wave probe 2) have little energy with $R_L < 2\%$. However, the results show that the ratio of R_L increases as the severity of waves increases. It may also grow up to 12% when the waves propagate to the berthing area. The reason for this is that dominant short waves may lose energy quickly while travelling from outside the port to the berthing region inside the port due to being affected by the north breakwater and other berthing structures, whereas long waves with lower energy are less affected by shelter structures and can maintain energy when propagating to the berthing site.

The estimated significant wave heights, as well as energy in long-period (low-frequency) zones, may aid in the safety of operation for tankers moored at the Leixoes oil terminal when compared to operational standards. However, no specific wave criteria for the oil terminal in Leixões are available in the literature. A value of $Z_s^{(\text{limit})} = 2.0$ m is found in the literature as a threshold for loading and unloading operations of moored tanker vessels between 30,000 and 200,000 DWT for waves acting longitudinally at the berthing site with direction $\pm 45^\circ$ of the longitudinal axis of the moored vessel (Puertos del Estado, 2011). OCDI (2020) recommends a critical significant wave height $Z_{sL}^{(\text{limit})} = 0.1$ m for cargo handling works at long wave period, applicable to ships whose surge resonant period is between 2 and 3 min. Hence, the threshold ratio of the low-frequency wave energy to the total wave energy at the berth can be defined as $R_L^{(\text{limit})} = 0.25$. The analysis of results reveals that, while the significant wave height criteria $Z_s^{(\text{limit})}$ are not exceeded in any test as depicted in Fig. 14(a), the criteria for the long-period wave energy ratio $R_L^{(\text{limit})}$ at the berth are exceeded across all tested wave conditions, as shown in Fig. 14(b).

Under different sea states, the waves were generated in a direction perpendicular to the extension of the north breakwater. However, they propagated inside the port, forming short-crested waves around the oil terminal's berthing site. A directional spectrum may help in finding the direction of short-crested waves. In this paper, the cross-power spectra between the available pairs are used to express the distribution of wave energy over frequency and propagation direction. The measured signals from an array of probes or ADV combined with a wave probe are used to estimate directional spectra at three different locations in the port, as

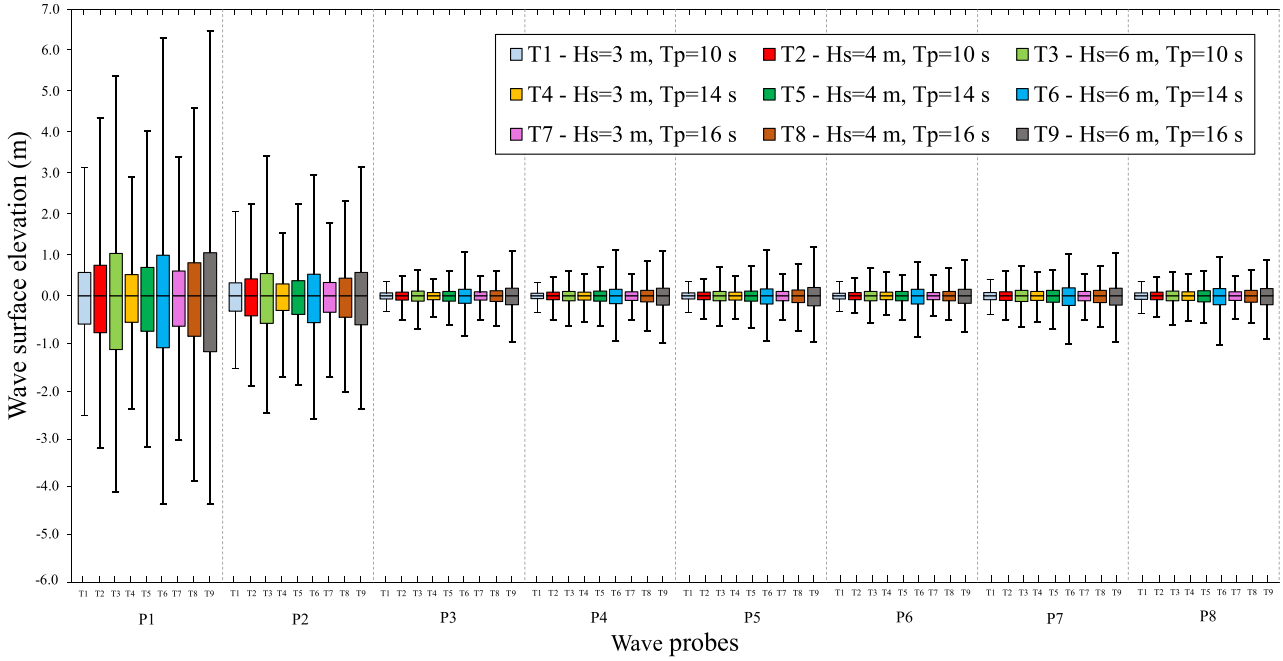

Fig. 13. Comparison of wave characteristics at each wave probe under various tested sea conditions.

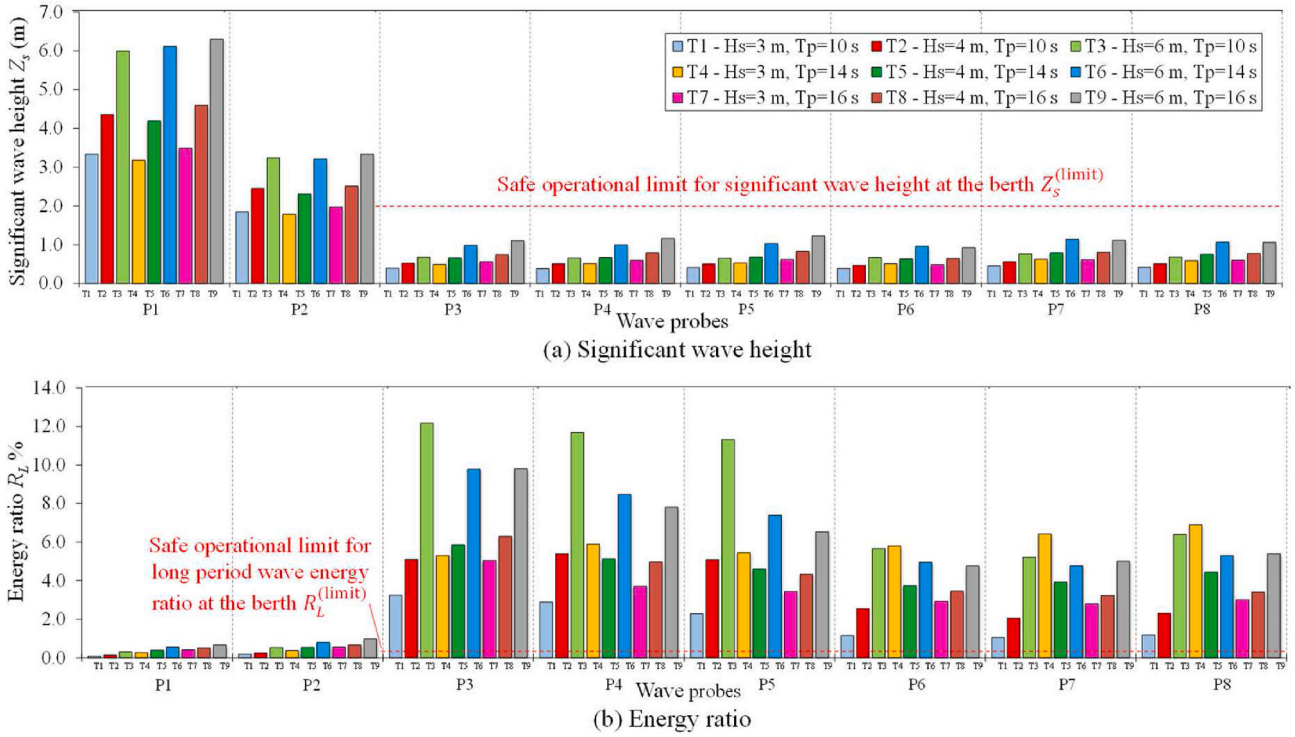

Fig. 14. Evolution of significant wave heights and energy ratio in the low-frequency band to total energy under various tested sea conditions.

explained in section 3.3.2. The calculations are performed using the directional wave spectra toolbox (DIWASP) version 1.4, which is based on the iterative maximum likelihood method IMLM (DIWASP, 2017).

Fig. 15 depicts an example of the estimated polar plots of the directional spectra at various sea conditions obtained by the array A installed in front of the ship's bow. The propagation direction is given relative to the ship's local axis (90° for waves coming from the starboard side and 180° refers to bow waves). Based on their propagation direction, the waves are classified as an incident or reflected. The dominant direction is defined based on the direction of the highest integrated energy across all frequencies. The polar plots show that as the wave period and height increase, the waves scatter less when they arrive at the berthing site. The analysis of results at Array A in front of the ship's bow shows that waves with heading angles between 216° and 221° may reach the berthing site at the tested sea states with $T_p = 10$ s. The heading, on the other hand, varies between 173° and 187° at the other tested sea states.

Table 7 displays the estimated significant wave heights and wave directions at three locations in the port under various tested wave conditions. The results show that the applied method for estimating directional spectra based on arrays of probes and ADV produces significant wave heights comparable to those obtained from individual probes in Fig. 14 at all tested sea states. In addition, the estimated wave directions obtained from two adjacent arrays (A and B) are similar, implying that the method provides accurate wave condition estimates. The analysis of results at three locations in the port at different sea states demonstrates how wave direction varies throughout the port. Waves generated perpendicular to the new extended breakwater reach probe 2 at the port entrance with directions ranging from 109° −112°, indicating that the waves diffract around the new breakwater's head. The waves then propagate to the berthing site, where they reach array A in front of the moored ship's bow with directions ranging from 173° −221° and array B near the moored vessel's mid-ship with directions between 191° and 215°. Finally, the results indicate that reflected waves may exist at the berthing site during the tested storms with heading angles between 334° and 10°. The study of the waves across the port of Leixões highlights the importance of describing wave conditions not only with wave heights and periods but also with directional spectra to account for all potential interactions around the berthing site.

4.2. *Influence of sea severity on operability*

Various sea conditions outside the port were examined to investigate the relationship between the ship responses and mooring loads with the joint distribution of significant wave heights H_s and peak wave periods T_p. The investigation spans a test duration of 3 h on the real scale. The moored ship's responses at the centre of gravity in 6 DOF are decomposed and referenced relative to the ship's equilibrium position. The outcomes are analysed in the time and frequency domains to determine the characteristics of linear and angular motions at various sea conditions. In the results that follow, all values are represented in real scale, unless specified. Table 8 presents a summary of the surge characteristics observed for a highly tensioned moored ship under various sea conditions. The results indicate a strong agreement between the significant peak-to-peak surge amplitudes calculated in the time domain using the zero-crossing technique and the significant spectral amplitudes, which represent the total energy. The modified box-whisker plots illustrating the characteristics of full-scale responses under various sea conditions are displayed in Fig. 16. Additionally, the figure includes information about the percentage of change in motion amplitudes resulting from the increase in wave heights. A negative surge denotes the ship moving towards the aft, while a negative sway signifies lateral movement away from the berth.

The results across different sea states reveal that skewness and kurtosis for responses in 6 DOF are close to 0 and 3.0, respectively. These values suggest that the probability distribution of the responses may fit a normal distribution. Furthermore, the findings show that as sea severity increases, all ship motions increase, especially for motions in the horizontal plane. Despite testing at lower wave heights, longer wave periods result in pronounced significant motion amplitudes. The results presented in Fig. 16 indicate that test number 3 yields the largest increase in response amplitudes, in terms of percentage, due to an increase in wave

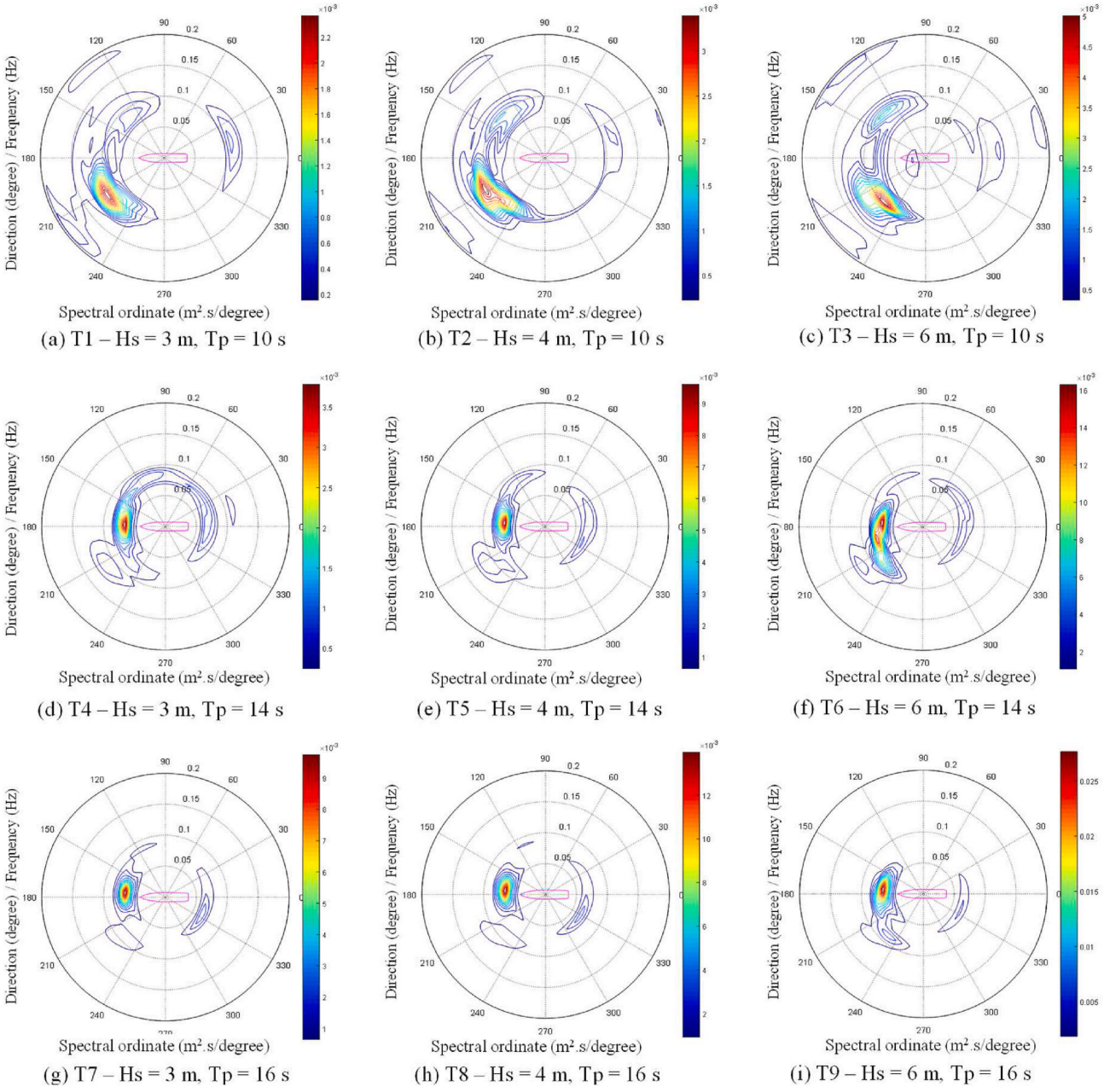

Fig. 15. Polar plot of directional wave spectra obtained from the array (A) at different sea states.

Table 7
Estimated wave directions in full scale at various locations and sea conditions.

Wave property	Unit	Location	Test condition								
			T1	T2	T3	T4	T5	T6	T7	T8	T9
Significant wave height	m	ADV + P2	1.85	2.39	3.22	1.78	2.29	3.20	1.98	2.52	3.34
		Array (A)	0.38	0.49	0.62	0.44	0.60	0.89	0.52	0.66	0.98
		Array (B)	0.37	0.45	0.61	0.46	0.59	0.89	0.46	0.59	0.82
Dominant incident wave direction	°	ADV + P2	111	112	112	111	112	113	109	111	112
		Array (A)	216	217	221	178	175	187	173	174	177
		Array (B)	215	216	208	199	193	196	191	194	194
Dominant reflected wave direction	°	Array (A)	14	15	14	11	10	21	337	334	351
		Array (B)	351	342	355	350	26	355	30	27	24

Table 8
Characteristics of surge motion at various sea states.

Motion properties	Units	Evaluated sea condition								
		T1	T2	T3	T4	T5	T6	T7	T8	T9
A_{max}	m	0.255	0.564	1.904	0.550	1.213	2.072	0.703	1.065	1.817
A_{min}	m	0.276	0.621	1.560	0.537	1.110	2.428	0.542	0.882	1.598
Skewness	–	0.058	0.165	0.320	0.155	0.220	−0.207	0.209	0.242	0.155
Kurtosis	–	3.266	3.547	2.944	3.001	3.649	3.637	3.511	3.275	3.349
Z_{avg}	m	0.114	0.298	1.284	0.288	0.544	1.393	0.285	0.525	1.072
Z_{max}	m	0.397	0.812	3.128	0.886	1.661	3.803	0.998	1.644	3.073
$Z_{1/3}$	m	0.307	0.634	2.283	0.643	1.165	2.648	0.641	1.162	2.205
Z_s	m	0.308	0.635	2.287	0.638	1.169	2.641	0.647	1.182	2.238
T_p	s	97.08	98.59	107.72	94.45	94.76	121.52	109.11	112.30	108.21
Z_{sL}	m	0.305	0.633	2.285	0.629	1.162	2.636	0.634	1.171	2.229
T_{pL}	s	97.08	98.58	107.72	94.45	94.76	121.52	109.11	112.30	108.21
R_L	–	98.098	99.292	99.830	97.083	98.722	99.601	95.938	98.165	99.216
Z_{limit}	m	3								
N stops	–	0	0	10	0	0	17	0	0	11
Downtime	s	0	0	82.427	0	0	332.36	0	0	100.58
operability	%	100	100	99.2	100	100	96.78	100	100	99.0

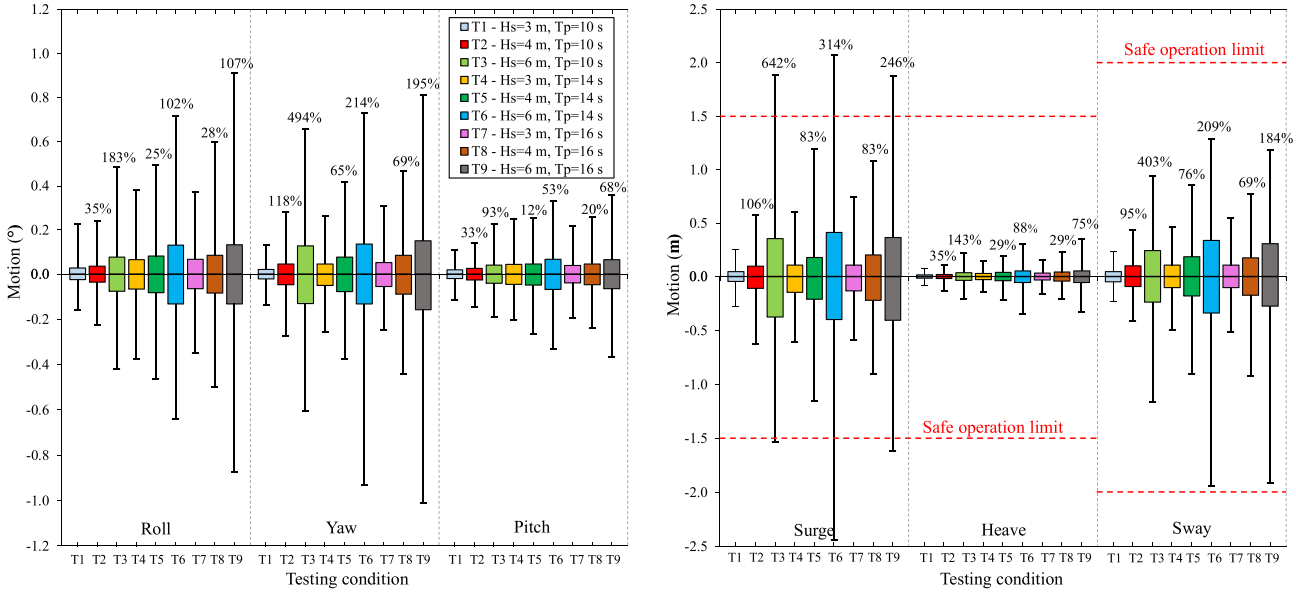

(a) Angular motions (b) Linear motion

Fig. 16. Response characteristics in 6 DOF for the highly tensioned moored case at various sea conditions.

height. The surge and sway motions exhibit the largest response amplitudes at a peak period of $T_p = 14$ s and a significant height $H_s = 6$ m. The surge motion stands out with a maximum peak-to-peak amplitude $Z_{max}^{\text{surge}} = 3.8$ m, consistently surpassing the defined safe operation limits for a moored tanker across all tested wave conditions with significant heights of $H_s = 6$ m. In this scenario, the surge motion exceeded the criteria 17 times, resulting in 333 s of downtime and an operational efficiency of 96.7%. Notably, both the significant Z_s^{surge} and mean Z_{avg}^{surge} amplitudes of the surge motions remain below the prescribed limits. Conversely, heave and sway motions exhibit maximum amplitudes of $Z_{max}^{\text{heave}} = 0.5$ m and $Z_{max}^{\text{sway}} = 3.1$ m, respectively, which both fall within the defined operational threshold. However, it is worth noting that the sway motion comes closer to approaching the limiting criteria. The pitch motion records the lowest angular motion with a maximum peak-to-peak amplitude of $Z_{max}^{\text{pitch}} = 0.63°$. On the other hand, roll and yaw exhibit the highest angular motions, with maximum amplitudes of $Z_{max}^{\text{roll}} = 1.6°$ and $Z_{max}^{\text{yaw}} = 1.8°$, respectively. It is important to note that these values remain within the operational limits.

Another crucial factor for assessing the safety of a moored ship under various sea conditions is the loads on mooring lines and fenders. The loads are characterized by zero-peak amplitudes in the recorded time series of loads as shown in Table 9. Results show a correlation between mean loads and pretension values in each mooring element. The minimum recorded load is zero when the mooring line becomes slack, or the ship moves away from the fender. The probability distribution of the load in each mooring element deviates from the normal distribution in terms of skewness and kurtosis, which can be caused by non-linear influences in the mooring system and non-linear wave ship interaction.

The analysis of mooring load spectra (not included) at various pretensions reveals that the mooring system's natural period corresponds to a high peak period. In general, testing under various sea conditions demonstrates that all mooring loads increase as wave height increases. The highest zero-peak load amplitude in the breast stern line $A_{max}^{\text{L3}} = 743$ kN at a significant wave height of 6 m and a peak period of 14 s exceeds the load failure criteria presented by the OCIMF (2018) at low pretensions. The discussion above demonstrates that the ship cannot operate safely at the oil terminal in the rough sea conditions because of the excessive surge motion and load in the breast stern mooring line 3. A different mooring configuration may, however, enhance operability.

Table 9
Characteristics of mooring loads at peak period $T_p = 14$ and significant wave height $H_s = 6$.

Load characteristics	Units	Line1	Line 2	Line 3	Line 4	Fender 1	Fender 2
A_{mean}	kN	235.4	138.0	143.5	234.0	261.0	266.5
Skewness	–	0.2	1.4	1.8	0.5	1.6	1.5
Kurtosis	–	4.3	5.7	7.4	3.4	6.5	6.1
A_{min}	kN	70.5	0.0	0.0	21.2	25.9	0.0
A_{max}	kN	504.1	621.6	743.1	613.6	1753.3	2057.6
A_s	kN	335.1	310.0	339.1	398.4	723.5	833.6
T_p	s	73.5	81.7	73.5	73.0	80.4	74.1
R_L	–	96.4	95.3	88.7	93.3	95.3	94.7
A_{limit}	kN	640	640	640	640	2450	2450

Response spectra are used to calculate the peak periods of the moored tanker's motions. The results are then compared to the calculated peak wave periods in section 4.1. Fig. 17 shows the full-scale estimated response spectra in 6 DOF for highly tensioned mooring lines at various sea states. The results show that, while the energy distributions spiked at various frequencies in the response spectra, dominant frequency peaks can be defined as mentioned in section 3.5.2. However, the oscillation periods associated with those dominant frequency peaks varied depending on the vessel's response. The values obtained at tested waves with $H_s = 6$ m and $T_p = 14$ s, for example, are as follows: $T_{\text{roll}} = 13.4$ s, $T_{\text{yaw}} = 62.9$ s, $T_{\text{pitch}} = 12.6$ s, $T_{\text{surge}} = 121.5$ s, $T_{\text{heave}} = 15.7$ s, and $T_{\text{sway}} = 63.4$ s.

These values are comparable to the full-scale natural periods determined by decay tests. The similarity between the sway and yaw oscillation periods highlights the close coupling between them. In general, the results in Fig. 17 show that the dominant frequencies for vertical plane motions correspond to shorter periods than those for horizontal plane motions. Low-frequency waves near the berthing site can therefore greatly excite surge, sway, and yaw motions. The peak periods of incident sea waves, on the other hand, have a significant impact on the oscillation periods for heave, pitch, and roll responses. Furthermore, the presence of spikes in the response spectrum of a specific mode of motion at natural frequencies corresponding to other modes of motion emphasises the effects of motion coupling.

Although the energy ratio in the low-frequency band of the wave spectra R_L^{wave} is less than 2% outside the port and up to 12% near the berthing site, at certain sea states, the energy ratio in the low-frequency band of the response spectra R_L^{motion} can reach high levels ranging from 56% to 99.8% for horizontal plane motions and up to 73% for heave motion. The heave-surge coupling is most likely causing the high energy ratios in heave motion. These findings demonstrate the significance of long wave energy around the berthing site on moored ship motions and cargo handling operations. In addition, it highlights the significance of incorporating low-frequency forces and coupling effects into numerical models to accurately estimate motions in waves for moored ships inside ports.

4.3. Influence of mooring pretension on operability

At low pretensions, the mono-parametric downtime assessment reveals motion and load limits that have been exceeded, as depicted in Fig. 18. The estimated downtimes due to surge and yaw motions are 354 and 56 s, respectively. In this section, the impact of various pretension conditions on the dynamic responses of the moored tanker in 6 DOF and mooring loads are analysed. Two different pretension configurations are examined as explained in section 3.4. Fig. 19 illustrates how, under various sea states, the mooring system's characteristics influence peak-to-peak response amplitudes in 6 DOF. The results are also compared with safe operation limits of motions as follows $Z_{limit}^{\text{surge}} = 3.0$ m, $Z_{limit}^{\text{sway}} = 4.0$ m, $Z_{limit}^{\text{heave}} = 3.0$ m, $Z_{limit}^{\text{roll}} = 2.0^\circ$, $Z_{limit}^{\text{pitch}} = 2.0^\circ$ and $Z_{limit}^{\text{yaw}} = 2.0^\circ$ (Elzinga et al., 1992; PIANC, 1995; Van der Molen, 2006).

Although the applied pretensions have a minor effect on the roll natural period as shown in Table 3, results in Fig. 19 show that the amplitudes of the roll indicate sensitivity to the applied pretensions, particularly at wave peak period $T_p = 14$ s. This is justified by the fact that high pretensions assist fenders in activating additional damping forces on the ship side, which aid in reducing the maximum and significant roll amplitudes (up to 24% and 16%, respectively), especially at a tested peak period close to the roll natural period and in the presence of a tiny potential damping force. The coupling between yaw and roll motions as well as the fenders effect on the side may explain similar reductions in maximum and significant yaw amplitudes (up to 30%) due to the increase in pretension values. The yaw reduction helps to prevent ten instances of exceeding the limits and a total downtime of 56 s, which leads to boost operability from 99.5% at low pretensions to full operability at higher pretensions allowing the ship to stay safe at the berth under severe wave conditions, as shown in Table 10.

The maximum and significant heave amplitudes may noticeably decrease by 17% and 15.5%, respectively, as pretensions rise. The impact of pretensions, however, is less obvious on pitch motion. Results show the energy ratios in the low-frequency band of all motions and loads do not significantly change with the pretension rises. However, they increase with the increase of wave heights. The amplitudes of the surge motion remained relatively unchanged despite an increase in the applied pretensions. This can be attributed to the ship's inability to reach close contact with fenders that generate sufficient longitudinal frictional forces to minimize surge motion. The ship side was subjected to high reactive fender loads on the other side due to the pretension rise, which increased sway motions.

Although the applied thresholds for the energy ratio of the long-period waves $R_L^{(\text{limit})}$ at the berth are exceeded under all tested sea states, as depicted in Fig. 14(b), the motion results in Fig. 19 show that the berthed vessel may experience unsafe surge or yaw motions during specific tests such as T3, T6 and T9. Consequently, the applied criterion for the significant wave height of the long-period waves $Z_{sL}^{(\text{limit})}$ may represent a conservative value for operation at the berth during these tests, particularly when observing that the critical significant wave height $Z_s^{(\text{limit})}$ at the berth is never exceeded in any test as shown in Fig. 14(a). This result emphasises the significance of adapting berthing site-specific criteria.

Increasing pretensions may have an impact on the clearance between the maximum motion amplitudes and operation thresholds, but it is also important to note that pretensions significantly influence the amplitudes of mooring loads, which must be also compared with the corresponding safety limits. Fig. 20 shows examples of downtime assessment based on the recorded time series for loads at high pretensions. The impact of mooring pretensions on maximum and significant zero-peak loads obtained in mooring elements during model testing under various sea conditions while accounting for the safety standards is shown in Fig. 21.

Results show that zero-peak load amplitudes in stern line 4 are less influenced by changes in pretension configuration while the other mooring elements are significantly affected by pretension effects. The maximum zero peak load amplitudes in both breast lines 2 and 3 may increase by 175% due to the increase in pretension. Therefore, not only

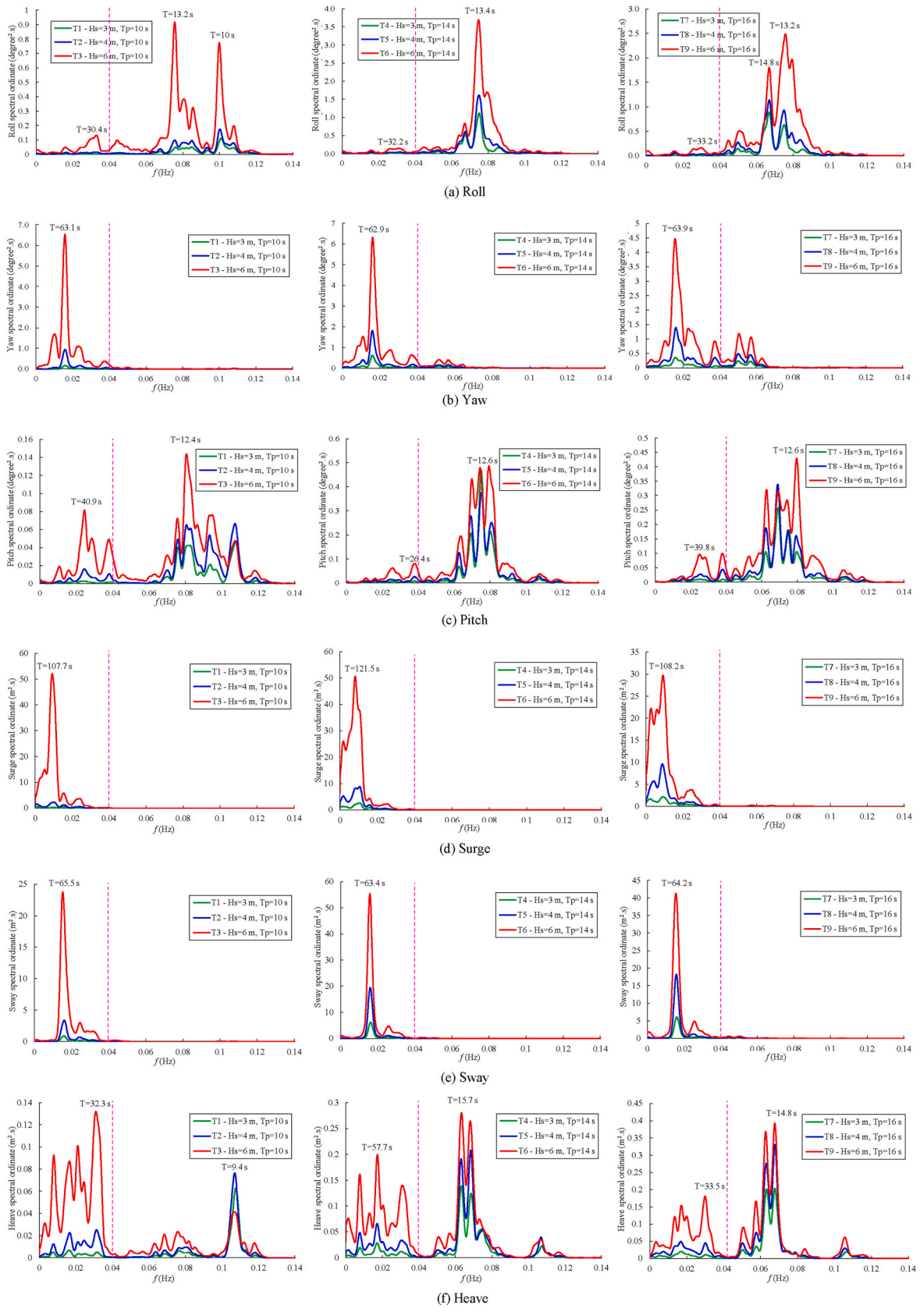

Fig. 17. Response spectra in 6 DOF obtained by Welch's method at various sea conditions.

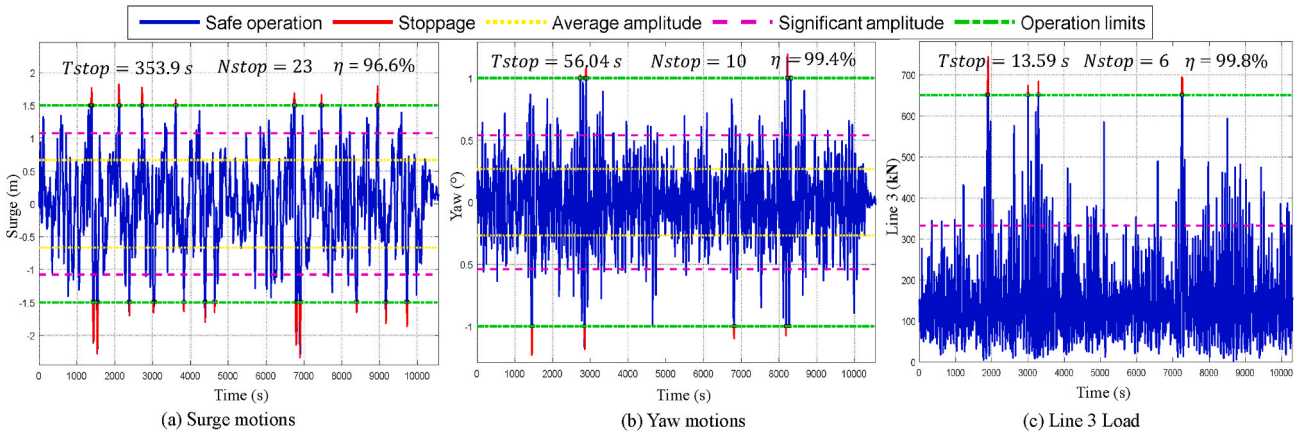

Fig. 18. Downtime analysis based on motions and loads at T_p = 14 s and H_s = 6 m with low pretensions.

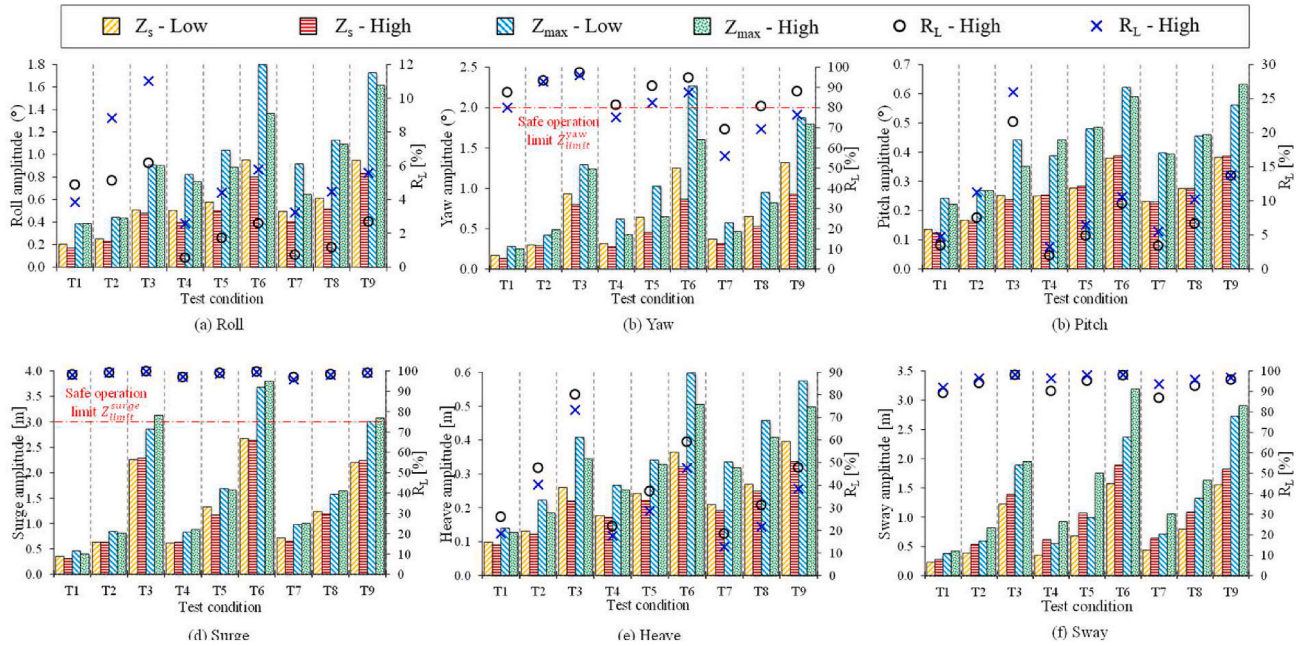

Fig. 19. Effect of pretension on ship response in 6 DOF under various wave conditions.

maximum zero-peak amplitudes but also significant zero-peak amplitudes exceed the failure criteria. Also, both fenders were much deflected at higher pretensions, increasing the maximum zero peak loads on fenders by up to 150% of the initial value. The number of stoppages caused by exceeding the load in lines 2 and 3 could reach 50 and 90, respectively, resulting in downtimes of 702 and 341 s and operability of 96.7% and 93.16%.

The observations from a mono-parametric downtime assessment at two pretension configurations under various sea conditions are summarized in Table 10. The results show that surge and yaw motions, as well as mooring load in the breast stern line 3, define the stoppage modes at low pretensions. The stoppage modes at higher pretensions are limited to surge motion and mooring loads in lines 1, 2 and 3 and fenders 1 and 2. The analysis of results depicted in Fig. 19(b) and Table 10 at low pretensions for yaw motion in test 9 and surge motion in test 3 reveals that the maximum peak-to-peak amplitudes ($Z^{yaw}_{max} = 1.87°$ and $Z^{surge}_{max} = 2.85$ m) are already below the corresponding threshold, whereas the zero-peak amplitudes ($A^{yaw}_{max} = 1.04°$ and $A^{surge}_{max} = 1.96$ m) may exceed the limits. This emphasises the significance of using the zero-peak amplitudes in conjunction with the maximum peak-to-peak amplitudes to acquire an accurate assessment of downtime and operability. The analysis of results shows that higher pretensions aided in mitigating yaw motion stoppage. However, it causes additional stoppage modes on the other side due to extreme loads on mooring lines 1 and 2, as well as fenders 1 and 2.

Although increasing pretensions assisted fenders in activating additional damping forces on the ship side, the increased pretension in general did not enhance the overall operability of the moored tanker. The reason could be the high percentage of increase in the pretensions or the inadequacy of the initial mooring plan. In addition, stiffness modification can be examined to improve overall operability by reducing motions while keeping mooring loads below safe limits.

5. Conclusions

This study investigates experimentally the effects of offshore maritime conditions and pretension configurations on the operability of a moored tanker ship at a newly modified berthing site inside a port. The physical model was constructed to replicate a new layout of the port of Leixões in Portugal, including bathymetry and a future 300 m extension of Leixões' outer breakwater. A tanker model was tested under a variety of offshore sea states and pretension configurations over a 3-h storm

Table 10
Downtime assessment at various wave conditions and pretension configurations based on zero-peak amplitudes of motions and loads.

Downtime source	Test	Downtime (s)		Number of stops		Operability (%)	
		Low-PT	High-PT	Low-PT	High-PT	Low-PT	High-PT
Yaw	T6	56.04	–	10	–	99.47	100
	T9	7.01	–	3	–	99.93	100
Surge	T3	143.22	82.43	8	10	98.61	99.20
	T6	353.89	332.36	23	17	96.65	96.78
	T9	74.08	100.58	7	11	99.28	99.02
Line 1	T3	–	3.99	–	2	100	99.96
	T6	–	8.95	–	7	100	99.91
	T9	–	3.65	–	2	100	99.96
Line 2	T3	–	305.44	–	27	100	97.05
	T6	–	341.02	–	50	100	96.70
	T8	–	5.74	–	1	100	99.94
	T9	–	295.54	–	37	100	97.13
Line 3	T3	–	246.66	–	6	100	97.61
	T5	–	2.59	–	1	100	99.97
	T6	13.59	431.33	6	64	99.87	95.82
	T8	–	27.18	–	9	100	99.74
	T9	8.03	702.97	2	90	99.92	93.16
Fender 1	T6	–	25.63	–	5	100	99.75
Fender 2	T6	–	27.10	–	5	100	99.74
	T9	–	83.64	–	16	100	99.19

duration in full scale. The applied physical modelling study is recommended to investigate the moored ship problem in severe waves at modified port terminals.

With the propagation of waves to the berthing area, the energy ratio at low frequencies reaches 12%, indicating the presence of long-period waves near the oil tanker's berthing site. The newly extended north breakwater contributes significantly to the reduction of the maximum and the significant wave heights, which reach up to 4.6 and 3.3 m at the port entrance, respectively. Within the berthing area of the oil terminal, they reach up to 1.8 and 1.2 m, respectively, during severe wave conditions. This is a noteworthy decrease in wave heights compared to data from previous studies, i.e., without the new breakwater extension. The modifications may, however, be less effective against long waves.

Short-crested spectral analysis helps to describe wave directions that influence the moored ship response at the berthing site. Results show that waves scatter less as the severity of the waves increases, reaching the ship's bow at the berthing site with angles ranging from 173° to 221°. Furthermore, reflected waves may exist at the berthing site. High energy ratios in the low-frequency band of horizontal plane response spectra illustrate the significance of long waves observed near the berthing site on ship motions, even if the energy ratio of the long-period waves is less than 2% outside the port and up to 12% near the berthing site. Although all examined sea states exceeded the operating criteria for this wave energy ratio at the berth, only three tests resulted in unsafe surge or yaw motions for the berthed vessel. Since the critical significant wave height of short waves at the berth is never exceeded in any test, the applied standard criterion for the significant wave height of the long-period waves may not be adequate for this berth site, highlighting the need for site-specific wave criteria. The measured wave conditions near the berth may aid in providing specific limiting criteria for short and long waves to enhance the safety of operation for moored tankers at the Leixões oil terminal.

In comparison to the conventional devices typically employed in most testing facilities for the physical modelling of real mooring systems, the custom-made mooring system simulators introduced in this study represent a potentially cost-effective alternative.

Although the pretension values in mooring lines and fenders were raised by 35–225% of their initial values, only the yaw motions demonstrated improvement in operability, leaving and occasionally adding other stoppage modes caused by exceeding the surge and load limits with insufficient control. It is crucial to clarify that the applied mooring system is generic which may be initially insufficient to provide full operability for all motions and loads simultaneously. Hence, it can be inferred that increasing pretensions should not be used blindly as a countermeasure to enhance operability without first ensuring that the mooring arrangement is feasible for safe operation. In other words, a study of operability under various pretension loads could help in determining whether the initial mooring plan is practical or not.

This study applied a generic asymmetrical mooring arrangement of four mooring lines and two fenders. Based on a mono-parametric downtime analysis, the findings in this study show that surge motion, line 1, line 2, and line 3 loads, as well as fender 1 and fender 2 loads, are the determining factors of downtime at the oil terminal of Leixões port due restrictions on the cargo loading arm and breaking loads for mooring lines and fenders. Although amplitudes of these motions and loads exceeded the standard thresholds at severe sea conditions, cargo operations may not always be disrupted in practice, because exceeding the safety threshold does not necessarily result in the snapping of mooring lines. Distributing the measured loads on extra mooring lines may enhance operability by preventing mooring failure and reducing

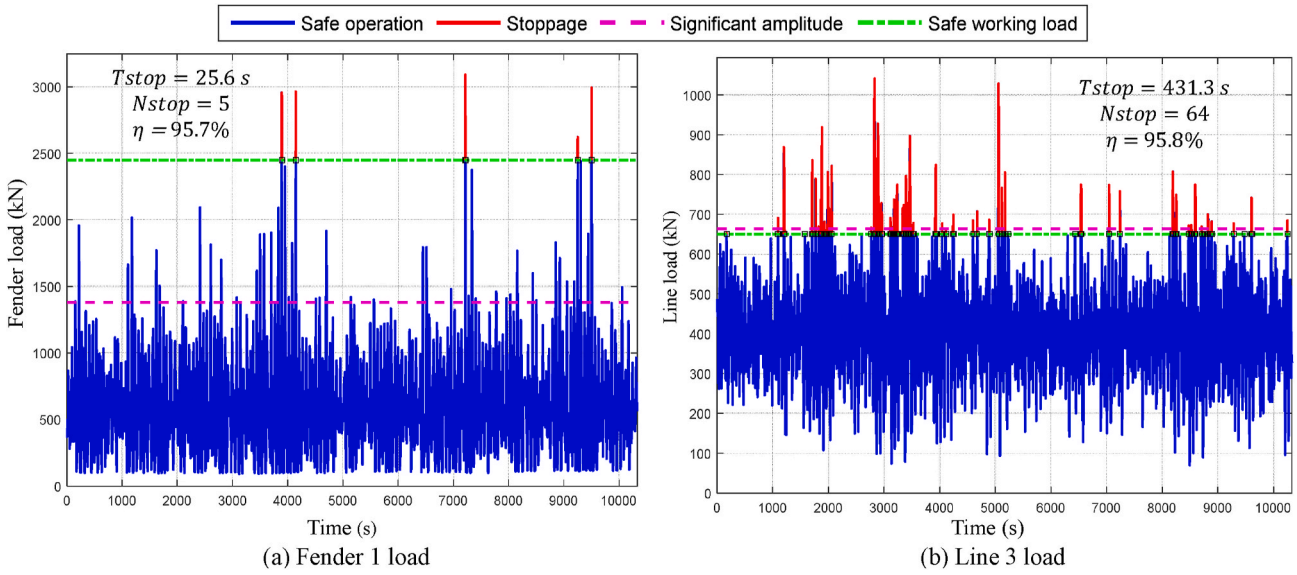

Fig. 20. Downtime analysis based on loads at $T_p = 14$ s and $H_s = 6$ m with high pretensions.

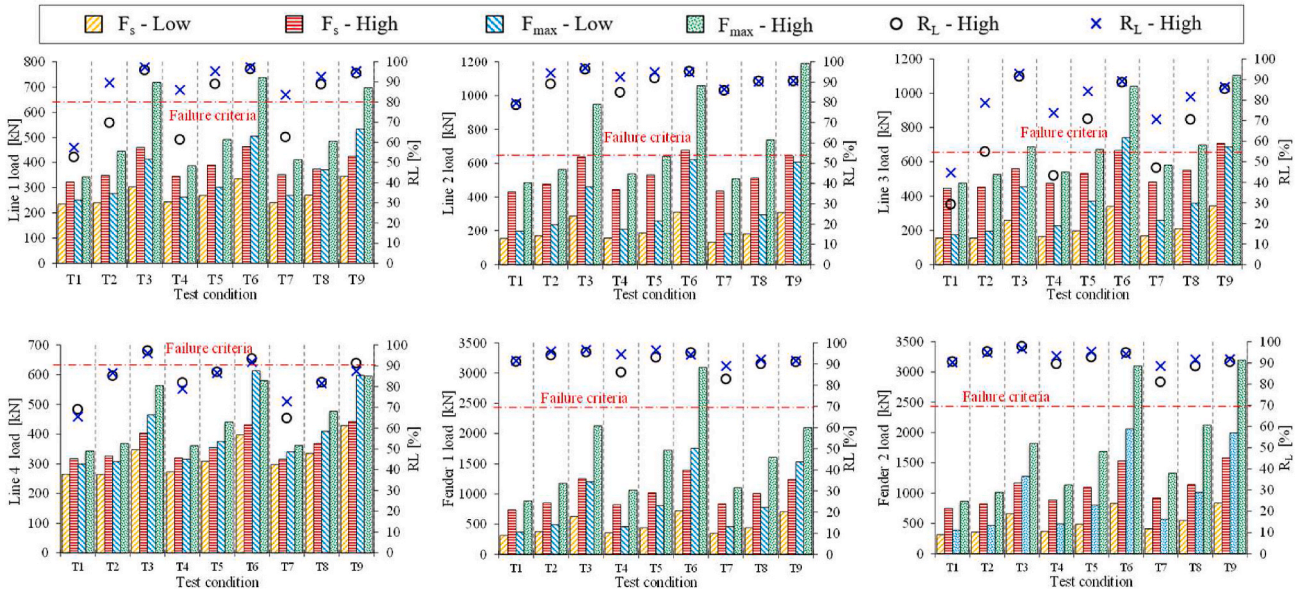

Fig. 21. Effect of pretension on mooring loads under various wave conditions.

the motions. Furthermore, various predictions of downtime and operability may be obtained by using more strict or loose motion/load criteria. Therefore, additional studies in the oil terminal of the port of Leixões with different ships may provide comparable results to this study, which could aid in specifying accurate limiting criteria for motions and loads specifically at the oil terminal rather than applying standard criteria.

The majority of published research only evaluated downtime using peak-to-peak amplitudes. Nevertheless, this study recommends zero-peak amplitudes to be used in conjunction with maximum peak-to-peak amplitudes to obtain accurate results for downtime and operability analysis. The applied operability analysis aids in determining the number and duration of expected stoppages, as well as the operational efficiency of the moored Esso Osaka tanker at the Leixoes oil terminal, which may be translated into technical and economic data that helps in the design and operation of the modified oil terminal.

The study concludes that the application of small-scale physical modelling for moored ships in port is a useful tool not only for investigating the feasibility of modifying port layouts within the existing sheltering structures but also for analysing additional soft countermeasures that may strengthen operational conditions at the berth area. In addition, the extensive experimental program and results presented in this study may aid in validating numerical models for the moored ship problem.

CRediT authorship contribution statement

H.S. Abdelwahab: Formal analysis, Visualization, Writing – original draft. **L. Pinheiro:** Writing – review & editing. **J.A. Santos:** Writing – review & editing. **C.J.E.M. Fortes:** Writing – review & editing. **C. Guedes Soares:** Writing – review & editing, Supervision.

Declaration of competing interest

The authors declare that they have no known competing financial interests or personal relationships that could have appeared to influence the work reported in this paper.

Data availability

No data was used for the research described in the article.

Acknowledgements

The experimental work in this paper was conducted within the scope of the M&M SHIPS project “Manoeuvring & Moored Ships in Ports” PTDC/EMSTRA/5628/2014) financed by the Portuguese Foundation for Science and Technology (Fundação para a Ciência e Tecnologia-FCT). The first author is funded by FCT for a PhD scholarship under contract 2020.06969.BD. This work contributes to the strategic research plan of the Centre for Marine Technology and Ocean Engineering (CENTEC), which is funded by FCT under contract UIDB/UIDP/00134/2020.

References

Abdelwahab, H.S., Guedes Soares, C., 2023. Experimental uncertainty of a physical model of a tanker moored to a terminal in a port. Mar. Struct. 87, 103331 https://doi.org/10.1016/j.marstruc.2022.103331.

Abdelwahab, H.S., Guedes Soares, C., Pinheiro, L.V., Fortes, C.J.E.M., Santos, J.A., 2021. Experimental and numerical study of wave-induced ship motions and mooring loads of a tanker moored in Leixões port. In: Guedes Soares, C., Santos, T.A. (Eds.), Developments in Maritime Technology and Engineering. Taylor & Francis Group, London, UK, pp. 341–350. https://doi.org/10.1201/9781003216599.

Ahuja, M.M., Mani, C.S., Joshi, A.K., 2010a. LNG berths for open seas: Part 1 Dahej LNG terminal, a case study. Port Technol. Int. 46, 119–123. URL. https://wpassets.porttechnology.org/wp-content/uploads/2019/05/25184022/119-123.pdf.

Ahuja, M.M., Mani, C.S., Joshi, A.K., 2010b. LNG berths for open seas: Part 2 Dahej LNG terminal, a case study. Port Technol. Int. 46, 125–129. URL. https://www.porttechnology.org/technical-papers/lng_berths_for_open_seas_dahej_lng_terminal_a_case_study_part_2/.

AMSA, 2015. Shaping shipping for people: thinking - mooring safety. URL. https://www.amsa.gov.au/sites/default/files/amsa282-maritime-safety-awareness-newsletter-sep-2015.pdf.

APDL, 2016. Request for submission of proposal. In: Physical and Numerical Model Studies of the Extension of the Outer Breakwater and the New Container Terminal at the Port of Leixões (in Portuguese). Portugal. https://www.apdl.pt/pt/descricao.

APDL, 2022. Extension of the outer breakwater of the port of leixões, deepening of the access channel and the rotation basin. URL. https://www.apdl.pt/projetos-investimentos/.

ASCE, 2014. Mooring of Ships to Piers and Wharves. American Society of Civil Engineers, Reston, VA. https://doi.org/10.1061/9780784413555.

Baker, S., Frank, G., Cornett, A., Williamson, D., Kingery, D., 2016. Physical modelling and design optimizations for a new container terminal at the port of moin, Costa Rica. In: Ports 2016. American Society of Civil Engineers, Reston, VA, pp. 560–569. https://doi.org/10.1061/9780784479919.057.

Bellotti, G., 2007. Transient response of harbours to long waves under resonance conditions. Coast. Eng. 54, 680–693. https://doi.org/10.1016/j.coastaleng.2007.02.002.

BHP, 2021. Port Hedland mooring management standard. URL. https://safety4sea.com/wp-content/uploads/2021/03/202105-Port-Hedland-Mooring-Management-Standard-FINAL.pdf.

Bingham, H.B., 2000. A hybrid Boussinesq-panel method for predicting the motion of a moored ship. Coast. Eng. 40, 21–38. https://doi.org/10.1016/S0378-3839(00)00002-8.

Capitão, R., Pinheiro, L.V., Fortes, C.J.E.M., 2017. Physical and numerical model studies of the lengthening of the outer breakwater and maritime accessibilities of leixões harbour, Study I - sea wave Regimes (Portuguese). Report No. 227, DHA/NPE, LNEC. Lisbon. URL. https://siaia.apambiente.pt/AIADOC/AIA3002/anx_acessibilidades_vol_iii_01_anexo_vii_rel_227_17_estudo i_reg de agit maritima2018528145139.pdf.

Cavotec, 2004. Automated mooring systems. URL. http://www.cavotec.com.ua/download/cat9/AMS.pdf.

Cornett, A., Wijdeven, B., Boeijinga, O.O., 2012. 3-D physical model studies of wave agitation and moored ship motions at Ashdod port. In: The 8th International Conference on Coastal and Port Engineering in Developing Countries COPEDEC, pp. 1–13. Chennai, India.

Costas, R., Figuero, A., Peña, E., Sande, J., Rosa-Santos, P., 2022. Integrated approach to assess resonance between basin eigenmodes and moored ship motions with wavelet transform analysis and proposal of operational thresholds. Ocean Eng. 247, 110678 https://doi.org/10.1016/J.OCEANENG.2022.110678.

Cummins, W.E., 1962. The impulse response function and ship motions. Schiffstechnik 9, 101–109.

De Bont, J., Van der Molen, W., Van der Lem, J., Ligteringen, H., Mühlenstein, D., Howle, M., 2010. Calculations of the motions of a ship moored with MoorMaster units. In: Proceedings of the 32nd PIANC International Navigation Congress. World Association for Waterborne Transport Infrastructure (PIANC), Liverpool, UK, pp. 622–635. URL. http://resolver.tudelft.nl/uuid:c1c4acb0-a626-4eae-8c2a-63e78d493137.

del Estado, Puertos, 2011. Recommendations for the Project and Execution in Docking and Mooring Works ROM 2.0-11 (Spanish). Ministry of Public Works, Madrid, Spain. https://www.puertos.es/es-es/BibliotecaV2/ROM_2.0-11.pdf.

Demenet, P.-F., Guisier, L., Marcol, C., 2018. Physical and numerical modelling of ships moored in ports. In: 34th PIANC World Congress. Curran Associates, Inc., Panama, pp. 214–227.

DIWASP, 2017. A Directional Wave Spectra Toolbox for MATLAB®: User Manual V1.1. Centre for Water Research, University of Western Australia.

DMAIB, 2020. Marine accident report on loss of control on Stone I. URL. https://dmaib.com/media/10212/stone-i-loss-of-control-of-on-4-january-2020.pdf.

DNV, 2020. A new look at safe mooring [WWW Document]. URL. https://www.dnv.com/expert-story/maritime-impact/A-new-look-at-safe-mooring.html.

Dobrochinski, J.P.H., 2014. A Combination of SWASH and Harberth to Compute Wave Forces on Moored Ships. Delft University of Technology.

Dobrochinski, J.P.H., van Deyzen, A., Zijlema, M., van der Hout, A., 2023. Combining numerical tools to determine wave forces on moored ships. Coast. Eng. 179, 104224 https://doi.org/10.1016/j.coastaleng.2022.104224.

Dong, G., Yan, M., Zheng, Z., Ma, X., Sun, Z., Gao, J., 2022. Experimental investigation on the hydrodynamic response of a moored ship to low-frequency harbor oscillations. Ocean Eng. 262, 112261 https://doi.org/10.1016/J.OCEANENG.2022.112261.

Elzinga, T., Iribarren, J.R., Jensen, O.J., 1992. Movements of moored ships in harbours. In: Edge, B.L. (Ed.), The 23rd Conference on Coastal Engineering. American Society of Civil Engineers ASME, Venice, Italy, pp. 3216–3229. URL. https://icce-ojs-tamu.tdl.org/icce/article/view/4924.

Esferra, R., Bernardino, J., Alfredini, P., 2018. Physical modeling applied in evaluation of the safety and efficiency of vessel mooring plans. Brazilian J. Water Resour. 23 https://doi.org/10.1590/2318-0331.231820170192.

Figuero, A., Rodríguez, Á.R., Sande, J., Peña, E., Rabuñal, J.R., 2018. Field measurements of angular motions of a vessel at berth : inertial device application. Control Eng. Appl. Informat. 20, 79–88.

Figuero, A., Sande, J., Peña, E., Alvarellos, A., Rabuñal, J.R., Maciñeira, E., 2019. Operational thresholds of moored ships at the oil terminal of inner port of A Coruña (Spain). Ocean Eng. 172, 599–613. https://doi.org/10.1016/j.oceaneng.2018.12.031.

Fortes, C.J.E.M., Lemos, R., Fortunato, A., Capitão, R., Pinheiro, L.V., Neves, M.G., Freire, P., Oliveira, F., Azevedo, A., Lopes, H., Tato, P., Brogueira Dias, E., Luís, L., 2017. Studies carried out to improve safety conditions maritime access to the port of leixões. In: Atas Das 9as Jornadas Portuguesas de Engenharia Costeira e Portuária - PIANC Portugal. APRH, Lisbon, p. 25. https://pianc.pt/wp-content/uploads/2021/03/9as-jornadas/22.pdf.

Fortunato, A.B., Freire, P., Oliveira, F.S.B.F., Azevedo, A., 2017a. Estudos em modelo físico e numérico do prolongamento do quebra-mar exterior e das acessibilidades marítimas do porto de Leixões, Estudo III – Avaliação dos impactes na dinâmica sedimentar. DHA/NPE, LNEC, Lisbon. Report No. 225.

Fortunato, A.B., Freire, P., Oliveira, F.S.B.F., Azevedo, A., Pinheiro, L., 2017b. Impacte do prolongamento do quebra-mar norte do porto de leixões na dinâmica sedimentar. In: Atas Das 9as Jornadas Portuguesas de Engenharia Costeira e Portuária - PIANC Portugal. APRH, Lisbon, p. 14.

Guedes Soares, C., 1984. Representation of double-peaked sea wave spectra. Ocean Eng. 11, 185–207. https://doi.org/10.1016/0029-8018(84)90019-2.

Guedes Soares, C., Rusu, L., Bernardino, M., Pilar, P., 2011. An operational wave forecasting system for the Portuguese continental coastal area. J. Oper. Oceanogr. 4, 17–27. https://doi.org/10.1080/1755876X.2011.11020124.

Himanen, L., 2016. Alternative Mooring Systems. Kymenlaakso University of Applied Sciences, Finland. URL. https://www.theseus.fi/bitstream/handle/10024/111541/Himanen_Laura.pdf?sequence=1&isAllowed=y.

Hughes, S.A., 1993. Physical models and laboratory techniques in coastal engineering. In: Advanced Series on Ocean Engineering, Advanced Series on Ocean Engineering. World Scientific Publishing, Singapore. https://doi.org/10.1142/2154.

Kim, Y.Y., Choi, K.-J., Chung, H., Han, S., Lee, P.-S., 2014. A ship-to-ship automatic docking system for ocean cargo transfer. J. Mar. Sci. Technol. 19, 360–375. https://doi.org/10.1007/s00773-014-0256-3.

Kim, S., Yu, Y., Lee, Y., 2019. A study on the allowable range of overhanging berthing at the port of Ulsan. J. Korean Soc. Mar. Environ. Saf. 25, 313–319. https://doi.org/10.7837/kosomes.2019.25.3.313.

Kubo, M., Saito, K., Sakakibara, S., Kitano, M., Sawada, M., 2001. A study on suitable mooring system for large and small ships under waves and wind. In: Coastal Engineering 2000, 27th International Conference on Coastal Engineering (ICCE). American Society of Civil Engineers, Reston, VA, pp. 3629–3642. https://doi.org/10.1061/40549(276)283.

Kumar, P., Zhang, H., Ik Kim, K., Yuen, D.A., 2016. Modeling wave and spectral characteristics of moored ship motion in Pohang New Harbor under the resonance conditions. Ocean Eng. 119, 101–113. https://doi.org/10.1016/j.oceaneng.2016.04.027.

Kwak, M., 2018. Numerical simulation of moored ship motion considering harbor resonance. In: Handbook of Coastal and Ocean Engineering. WORLD SCIENTIFIC, pp. 1081–1110. https://doi.org/10.1142/9789813204027_0037.

Kwak, M., Pyun, C., 2013. Computer simulation of moored ship motion considering harbor resonance in Pohang new harbor. In: Ports 2013, Proceedings. American Society of Civil Engineers, Reston, VA, pp. 1415–1424. https://doi.org/10.1061/9780784413067.145.

Lee, S.W., Sasa, K., Aoki, S. ich, Yamamoto, K., Chen, C., 2021. New evaluation of ship mooring with friction effects on mooring rope and cost-benefit estimation to improve port safety. Int. J. Nav. Archit. Ocean Eng. 13, 306–320. https://doi.org/10.1016/j.ijnaoe.2021.04.002.

Lemos, R., Neves, M.G., Fortes, C.J.E.M., 2017a. Physical and Numerical Model Studies of the Lengthening of the Outer Breakwater and Maritime Accessibilities of Leixões Harbour, Study I - Two-Dimensional Stability and Overtopping Tests. DHA/NPE, LNEC, Lisbon (in Portuguese). Report No 226.

Lemos, R., Neves, M.G., Fortes, C.J.E.M., 2017b. Physical and Numerical Model Studies of the Lengthening of the Outer Breakwater and Maritime Accessibilities of Leixões Harbour, Study I - Three-Dimensional Agitation and Stability Tests and Overtopping. DHA/NPE, LNEC, Lisbon (in Portuguese). Report No. 298.

Liu, D., Rong, H., Guedes Soares, C., 2023. Shipping route modelling of AIS maritime traffic data at the approach to ports. Ocean Eng. https://doi.org/10.1016/j.oceaneng.2023.115868.

López, M., Iglesias, G., 2014. Long wave effects on a vessel at berth. Appl. Ocean Res. 47, 63–72. https://doi.org/10.1016/j.apor.2014.03.008.

Lucas, C., Silva, D., Guedes Soares, C., 2023. Climatic directional wave spectra in coastal sites. Coast. Eng. 180, 104255 https://doi.org/10.1016/j.coastaleng.2022.104255.

Ma, Q.W., Yan, S., 2009. QALE-FEM for numerical modelling of non-linear interaction between 3D moored floating bodies and steep waves. Int. J. Numer. Methods Eng. 78, 713–756. https://doi.org/10.1002/nme.2505.

MAIB, 2017. Report on the Investigation of the Failure of a Mooring Line on Board the LNG Carrier Zarga. Southampton. https://assets.publishing.service.gov.uk/media/59400114e5274a5e4e000239/MAIBInvReport13_2017.pdf.

Marcos-Rita, M., 1984. On the Behaviour of Moored Ships in Harbors:theory, Practice and Model Tests. LNEC, Lisbon.

McComb, P., Johnson, D.L., Beamsley, B., 2009. Numerical Study of Options to Reduce Swell and Long Wave Penetration at Port Geraldton.

Molina-Sanchez, R., Campos, Á., de Alfonso, M., de los Santos, F.J., Rodríguez-Rubio, P., Pérez-Rubio, S., Camarero-Orive, A., Álvarez-Fanjul, E., 2020. Assessing operability on berthed ships. Common approaches, present and future lines. J. Mar. Sci. Eng. https://doi.org/10.3390/jmse8040255.

Montgomery, P.J., 2013. Automated Mooring Method and Mooring System. US8408153B2.

MSC, 2020a. Guidelines on the design of mooring arrangements and the selection of appropriate mooring equipment and fittings for safe mooring. URL. https://www.imo.org/en/OurWork/Safety/Pages/SafeMooring.aspx.

MSC, 2020b. Guidelines for inspection and maintenance of mooring equipment including lines. URL. https://www.imo.org/en/OurWork/Safety/Pages/SafeMooring.aspx.

MSC, 2020c. Revised guidance on shipboard towing and mooring equipment. URL. https://www.imo.org/en/OurWork/Safety/Pages/SafeMooring.aspx.

NTSB, 2018. Breakaway of Containership Helsinki Bridge and Subsequent Allision with Black Falcon Cruise Terminal. https://safety4sea.com/wp-content/uploads/2018/12/NTSB-Breakaway-of-containership-Helsinki-Bridge-and-subsequent-allision-with-black-falcon-cruise-terminal-2018_12.pdf.

OCDI, 2020. Technical Standards and Commentaries for Port and Harbour Facilities in Japan. The Overseas Coastal Area Development Institute of Japan, Tokyo, Japan. URL. https://ocdi.or.jp/tec_st/tec_pdf/tech_00H.pdf.

OCIMF, 2018. Mooring Equipment Guidelines: (MEG4). Witherby Seamanship International Ltd., London, UK. URL. https://www.ocimf.org/publications/books/mooring-equipment-guidelines-meg4.

PIANC, 1995. Criteria for Movements of Moored Ships in Harbours: a Practical Guide - A Practical Guide, Permanent Technical Committee II. Working Group No. 2 (Brussels, Belgium).

Pinheiro, L.V., Fortes, C.J.E.M., Abecassis Jalles, B.M., Santos, J.A., 2015. Simulation of wave action on a moored container carrier inside Sines' harbour. In: Guedes Soares, C., Santos, T.A. (Eds.), Maritime Technology and Engineering. Taylor & Francis Group, London, UK, pp. 1113–1121.

Pinheiro, L.V., Fortes, C.J.E.M., Neves, M.G., 2017a. Study I - Wave Study - Propagation of Long Waves to the Interior of the Port, with Numerical Model. DHA/NPE, LNEC, Lisbon (in Portuguese). Report No. 296.
Pinheiro, L.V., Fortes, C.J.E.M., Neves, M.G., 2017b. Study I - Resonance Study - Propagation of Long Waves to the Interior of the Port, with Numerical Model. DHA/NPE, LNEC, Lisbon (in Portuguese). Report No. 300.
Pinheiro, L.V., Fortes, C.J.E.M., Neves, M.G., 2017c. Study II — Evaluation of the Impacts of the Extension of the Outer Breakwater of the Port of Leixões in the Wave Conditions of the Beach of Matosinhos (in Portuguese). Report No. 306, DHA/NPE, LNEC. Lisbon. https://siaia.apambiente.pt/AIADOC/AIA3002/anx_acessibilidades_vol_iii_01_anexo_vii_rel_306_17_estudo ii_agitação praia2018528145148.pdf.
Pinheiro, L.V., Abdelwahab, H.S., Santos, J.A., Fortes, C., Guedes Soares, C., 2020a. Scale-model tests of a moored tanker at Leixões port with breakwater's extension. In: Proceedings of the Coastal Engineering Conference, p. 37. https://doi.org/10.9753/icce.v36v.structures.37.
Pinheiro, L.V., Francisco, P., Abdelwahab, H.S., Fortes, C.J.E.M., Santos, J.A., Capitão, R., 2020b. Leixões north breakwater extension: physical modelling of a moored ship at berth A. Rev. Recur. Hídricos 41, 17–28 in Portuguese. https://www.aprh.pt/rh/v41n1_cti-2.html.
PPA, 2021. Mooring line and mooring systems management. URL. https://www.pilbaraports.com.au/PilbaraPortsAuthority/media/Documents/Port_of Port Hedland/Safety and Security/Marine Safety Bulletins/2021/PH-01-2021-Mooring-Line-and-Mooring-Systems-Management.pdf.
Rijnsdorp, D.P., Zijlema, M., 2016. Simulating waves and their interactions with a restrained ship using a non-hydrostatic wave-flow model. Coast. Eng. 114, 119–136. https://doi.org/10.1016/j.coastaleng.2016.04.018.
Rijnsdorp, D.P., Wolgamot, H., Zijlema, M., 2022. Non-hydrostatic modelling of the wave-induced response of moored floating structures in coastal waters. Coast. Eng. 177, 104195 https://doi.org/10.1016/j.coastaleng.2022.104195.
Rosa-Santos, P.J., Taveira-Pinto, F., 2013. Experimental study of solutions to reduce downtime problems in ocean facing ports: the Port of Leixões, Portugal, case study. J. Appl. Water Eng. Res. 1, 80–90. https://doi.org/10.1080/23249676.2013.831590.
Rosa-Santos, P., Veloso-Gomes, F., Taveira-Pinto, F., Brógueira-Dias, E., Guedes-Lopes, H., 2008. Improving operational conditions at Leixões oil terminal – Portugal. In: The 7th International Conference on Coastal and Port Engineering in Developing Countries (COPEDEC VII), pp. 1–18. Dubai, United Arab Emirates.
Rosa-Santos, P., Veloso-Gomes, F., Taveira-Pinto, F., Brógueira-Dias, E., 2010. Physical modelling of Leixões oil terminal – Portugal. In: Port Infrastructure Seminar, pp. 1–15. Delft, Netherlands. https://repository.tudelft.nl/islandora/object/uuid:efe48f74-128d-486a-b1b3-da9a76c804b4/datastream/OBJ1/download.
Rosa-Santos, P., Taveira-Pinto, F., Veloso-Gomes, F., 2014. Experimental evaluation of the tension mooring effect on the response of moored ships. Coast. Eng. 85, 60–71. https://doi.org/10.1016/j.coastaleng.2013.11.012.
Rusu, E., Guedes Soares, C., 2011. Wave modelling at the entrance of ports. Ocean Eng. 38, 2089–2109. https://doi.org/10.1016/j.oceaneng.2011.09.002.
Rusu, L., Guedes Soares, C., 2013. Evaluation of a high-resolution wave forecasting system for the approaches to ports. Ocean Eng. 58, 224–238. https://doi.org/10.1016/j.oceaneng.2012.11.008.
Rusu, L., Pilar, P., Guedes Soares, C., 2008. Hindcast of the wave conditions along the west Iberian coast. Coast. Eng. 55, 906–919. https://doi.org/10.1016/j.coastaleng.2008.02.029.
Sakakibara, S., Kubo, M., 2007. Ship berthing and mooring monitoring system by pneumatic-type fenders. Ocean Eng. 34, 1174–1181. https://doi.org/10.1016/j.oceaneng.2006.07.006.
Sakakibara, S., Kubo, M., 2008a. Characteristics of low-frequency motions of ships moored inside ports and harbors on the basis of field observations. Mar. Struct. 21, 196–223. https://doi.org/10.1016/j.marstruc.2007.11.002.
Sakakibara, S., Kubo, M., 2008b. Effect of mooring system on moored ship motions and harbour tranquillity. Int. J. Ocean Syst. Manag. 1, 84. https://doi.org/10.1504/IJOSM.2008.017783.
Santos, T.A., Guedes Soares, C., 2017. Development dynamics of the Portuguese range as a multi-port gateway system. J. Transport Geogr. 60, 178–188. https://doi.org/10.1016/j.jtrangeo.2017.03.003.
Santos, J.A., Pinheiro, L.V., Abdelwahab, H.S., Fortes, C.J.E.M., Pedro, F.G.L., Capitão, R. P., Hinostroza, M.A., Guedes Soares, C., 2019. Physical modelling of motions and forces on a moored ship at the Leixões port. Defect Diffus. Forum 396, 60–69. https://doi.org/10.4028/www.scientific.net/DDF.396.60.
Shiraishi, S., 2009. Numerical simulation of ship motions moored to quay walls in long-period waves and proposal of allowable wave heights for cargo handling in a port. In: The 9th International Offshore and Polar Engineering Conference (Osaka, Japan).
Taveira-Pinto, F., Veloso-Gomes, F., Rosa-Santos, P., Guedes Soares, C., Fonseca, N., Santos, J.A., Paulo-Moreira, A., Costa, P., Brógueira-Dias, E., 2008. Analysis of the behavior of moored tankers. In: Proceedings of the International Conference on Offshore Mechanics and Arctic Engineering - OMAE. Estoril, Portugal, pp. 755–764. https://doi.org/10.1115/OMAE2008-58013.
TSB, 2018. Mooring accident: bulk carrier Nord Quebec. Gatineau. URL. https://www.tsb.gc.ca/eng/rapports-reports/marine/2017/m17c0060/m17c0060.pdf.
UK P&I Club, 2009. Understanding mooring incidents. URL. https://www.ukpandi.com/news-and-resources/bulletins/2009/understanding-mooring-incidents/.
UK P&I Club, 2016. Risk focus: moorings. URL. https://www.ukpandi.com/news-and-resources/bulletins/2016/risk-focus-mooring/.
Uzaki, K. ichi, Matsunaga, N., Nishii, Y., Ikehata, Y., 2010. Cause and countermeasure of long-period oscillations of moored ships and the quantification of surge and heave amplitudes. Ocean Eng. 37, 155–163. https://doi.org/10.1016/j.oceaneng.2009.12.004.
Van der Burg, G., 2011. ShoreTension: secured to shore at all times. Port Technol. Int. 52, 43–45. https://wpassets.porttechnology.org/wp-content/uploads/2019/05/25181924/PTI52-08.pdf.
Van der Molen, W., 2006. Behaviour of Moored Ships in Harbours. PhD, Delft University of Technology. URL. http://resolver.tudelft.nl/uuid:1c20fa4a-ee42-4236-a69b-b895a81413af.
Van der Molen, W., Wenneker, I., 2008. Time-domain calculation of moored ship motions in nonlinear waves. Coast. Eng. 55, 409–422. https://doi.org/10.1016/j.coastaleng.2008.01.001.
Van der Molen, W., Monárdez, P., van Dongeren, A., 2006. Numerical simulation of long-period waves and ship motions in tomakomai port, Japan. Coast Eng. J. 48, 59–79. https://doi.org/10.1142/S0578563406001301.
Van der Molen, W., Scott, D., Taylor, D., Elliott, T., 2016. Improvement of mooring configurations in Geraldton harbour. J. Mar. Sci. Eng. https://doi.org/10.3390/jmse4010003.
Van Deyzen, A., Lem, J., Beimers, P.B., de Bont, J., 2014. The effect of active motion dampening systems on the behaviour of moored ships by. In: 33rd PIANC World Congress, pp. 1–13. San Francisco, USA.
Van Deyzen, A., Beimers, P.B., Lem, J., Messiter, D., de Bont, J., 2015. To improve the efficiency of ports exposed to swell. In: Australasian Coasts & Ports Conference, pp. 1–8. Auckland, New Zealand.
Van Oortmerssen, G., 1976. The Motions of a Moored Ship in Waves. PhD, Delft University of Technology. URL. http://resolver.tudelft.nl/uuid:4ebf906e-fa3e-4508-bd33-349d389c3cae.
Van Reenen, W., 2013. Automatic magnetic mooring. In: 23rd Session of ADN Safety Committee (WP.15/AC.2), p. 34. URL. https://unece.org/DAM/trans/doc/2013/dgwp15ac2/Dock_lock_presentation_1.pdf.
Veloso-Gomes, F., Taveira-Pinto, F., Rosa-Santos, P., Brógueira-Dias, E., Guedes-Lopes, H., 2005. Berthing characteristics and the behaviour of the oil terminal of Leixões harbour. In: Maritime Heritage and Modern Ports. WIT Press, Portugal, pp. 481–492.
Villa-Caro, R., Carral, J.C., Fraguela, J.Á., López, M., Carral, L., 2018. A review of ship mooring systems. Brodogradnja 69, 123–149. https://doi.org/10.21278/brod69108.
Weiler, O., Cozijn, H., Wijdeven, B., Le-Guennec, S., Fontaliran, F., 2009. Motions and mooring loads of an LNG-carrier moored at a jetty in a complex bathymetry. In: Proceedings of the ASME 28th International Conference on Ocean, Offshore and Arctic Engineering OMAE, pp. 425–435. https://doi.org/10.1115/OMAE2009-79420. Honolulu, Hawaii.
Wenneker, I., Borsboom, M.J.A., Pinkster, J.A., Weiler, O.M., 2006. A Boussinesq-type wave model coupled to a diffraction model to wave-induced ship motion. In: 31st PIANC Congress. Estoril, Portugal.
Xiong, L., Lu, H., Yang, J., Zhao, W., 2015. Motion responses of a moored barge in shallow water. Ocean Eng. 97, 207–217. https://doi.org/10.1016/j.oceaneng.2015.01.018.
Yoneyama, H., Shiraishi, S., Satoh, H., 2004. Experimental verification of a reduction system for low-frequency ship motions and examination for its practical use. In: Oceans '04 MTS/IEEE Techno-Ocean '04 (IEEE Cat. No.04CH37600). IEEE, pp. 1121–1128. https://doi.org/10.1109/OCEANS.2004.1405667.
Zijlema, M., Stelling, G., Smit, P., 2011. SWASH: an operational public domain code for simulating wave fields and rapidly varied flows in coastal waters. Coast. Eng. 58, 992–1012. https://doi.org/10.1016/j.coastaleng.2011.05.015.